Quaternary Research (2018), **89**, 281–306.

doi:10.1017/qua.2017.92

Quantifying episodic erosion and transient storage on the western margin of the Tibetan Plateau, upper Indus River

Tara N. Jonell[a,b]*, Lewis A. Owen[c], Andrew Carter[d], Jean-Luc Schwenniger[e], Peter D. Clift[b]

[a]School of Geosciences, University of Louisiana at Lafayette, Lafayette, Louisiana 70504, USA
[b]Department of Geology and Geophysics, Louisiana State University, Baton Rouge, Louisiana 70803, USA
[c]Department of Geology, University of Cincinnati, Cincinnati, Ohio 45221, USA
[d]Department of Earth and Planetary Sciences, Birkbeck College, London WC1E 7HX, United Kingdom
[e]Research Laboratory for Archaeology and the History of Art, University of Oxford, Oxford OX1 3QY, United Kingdom

(Received April 13, 2017; Accepted September 27, 2017)

Abstract

Transient storage and erosion of valley fills, or sediment buffering, is a fundamental but poorly quantified process that may significantly bias fluvial sediment budgets and marine archives used for paleoclimatic and tectonic reconstructions. Prolific sediment buffering is now recognized to occur within the mountainous upper Indus River headwaters and is quantified here for the first time using optically stimulated luminescence dating, petrography, detrital zircon U-Pb geochronology, and morphometric analysis to define the timing, provenance, and volumes of prominent valley fills. This study finds that climatically modulated sediment buffering occurs over 10^3–10^4 yr time scales and results in biases in sediment compositions and volumes. Increased sediment storage coincides with strong phases of summer monsoon and winter westerlies precipitation over the late Pleistocene (32–25 ka) and mid-Holocene (~8–6 ka), followed by incision and erosion with monsoon weakening. Glacial erosion and periglacial frost-cracking drive sediment production, and monsoonal precipitation mediates sediment evacuation, in contrast to the arid Transhimalaya and monsoonal frontal Himalaya. Plateau interior basins, although volumetrically large, lack transport capacity and are consequently isolated from the modern Indus River drainage. Marginal plateau catchments that both efficiently produce and evacuate sediment may regulate the overall compositions and volumes of exported sediment from the Himalayan rain shadow.

Keywords: River; Terrace; Provenance; Himalaya; Indus; Monsoon; Zanskar

INTRODUCTION

Deep marine sediments represent the final sedimentary record delivered by river systems to the ocean. These sediments are the product of erosion and transport by fluvial systems from multiple source regions, and modified by deposition and erosion from terraces and floodplains during transport. As sediments are routed from their mountain sources to the final depocenter, transient storage and erosion, or sediment buffering, modulate erosional signals such that any propagated signal of erosion can be dampened or erased altogether (e.g., Castelltort and Van Den Driessche, 2003; Jerolmack and Paola, 2010; Armitage et al., 2011; Romans et al., 2016). The potential for significant buffering complicates the use of marine sedimentary archives for long-term reconstructions of erosion and paleoclimate at high resolution. Large uncertainties remain in our understanding of how buffering attenuates erosional signals and over what time scales this process may be significant in source-to-sink transport systems (e.g., Goodbred, 2003; Clift, 2006; Allen, 2008; Armitage et al., 2011; Simpson and Castelltort, 2012).

Sediment budgets attempting to characterize buffering in large river systems have principally focused on quantifying storage and erosion of deposits in extensive floodplains (Allison et al., 1998; Métivier and Gaudemer, 1999; Castelltort and Van Den Driessche, 2003). Only recently in the Himalayan Indus and Ganges-Brahmaputra rivers has the capacity for substantial buffering in mountain source regions, as well as in the foreland basin, been recognized (Blöthe and Korup, 2013; Clift and Giosan, 2014). Across the Himalaya, wide (>5 km), glacially scoured, and overdeepened intermontane river basins provide exceptional accommodation space for sediment storage (Owen et al., 2006; Korup et al., 2010; Bolch et al., 2012; Blöthe and Korup, 2013). Thick alluvial river terrace sequences document considerable storage and release of sediment on shorter,

*Corresponding author at: School of Geosciences, University of Louisiana at Lafayette, Lafayette, Louisiana 70504, USA. E-mail address: tara.jonell@louisiana.edu (T.N. Jonell).

climate-relevant time scales (Bookhagen et al., 2006; Srivastava et al., 2008; Blöthe et al., 2014; Scherler et al., 2015; Dey et al., 2016; Munack et al., 2016).

Although local valley sediment storage and evacuation is evident, it is unclear what processes control the storage and release of material from these valleys. Tectonic forcing can be significant over longer geologic time scales (>10^6 yr), but here we examine the role of climate in modulating storage and release of sediment on shorter time scales. In particular, this study focuses on the relative importance of glaciation and precipitation provided by the Asian summer monsoon and winter westerlies in the northwest Himalaya. Although the mechanisms for storage and release of sediment have been investigated in the wetter monsoonal, south-facing front of the Himalaya (e.g., Bookhagen et al., 2006), it is less clear what processes influence sediment production and transport on the edge of the Tibetan Plateau in the Himalayan rain shadow where dramatic, large volume valleys fills are preserved (Blöthe and Korup, 2013; Hedrick et al., 2017).

In this study, alluvial terraces are investigated in the Zanskar River basin, the largest tributary (14,939 km^2) discharging to the upper Indus River (Fig. 1), to evaluate the

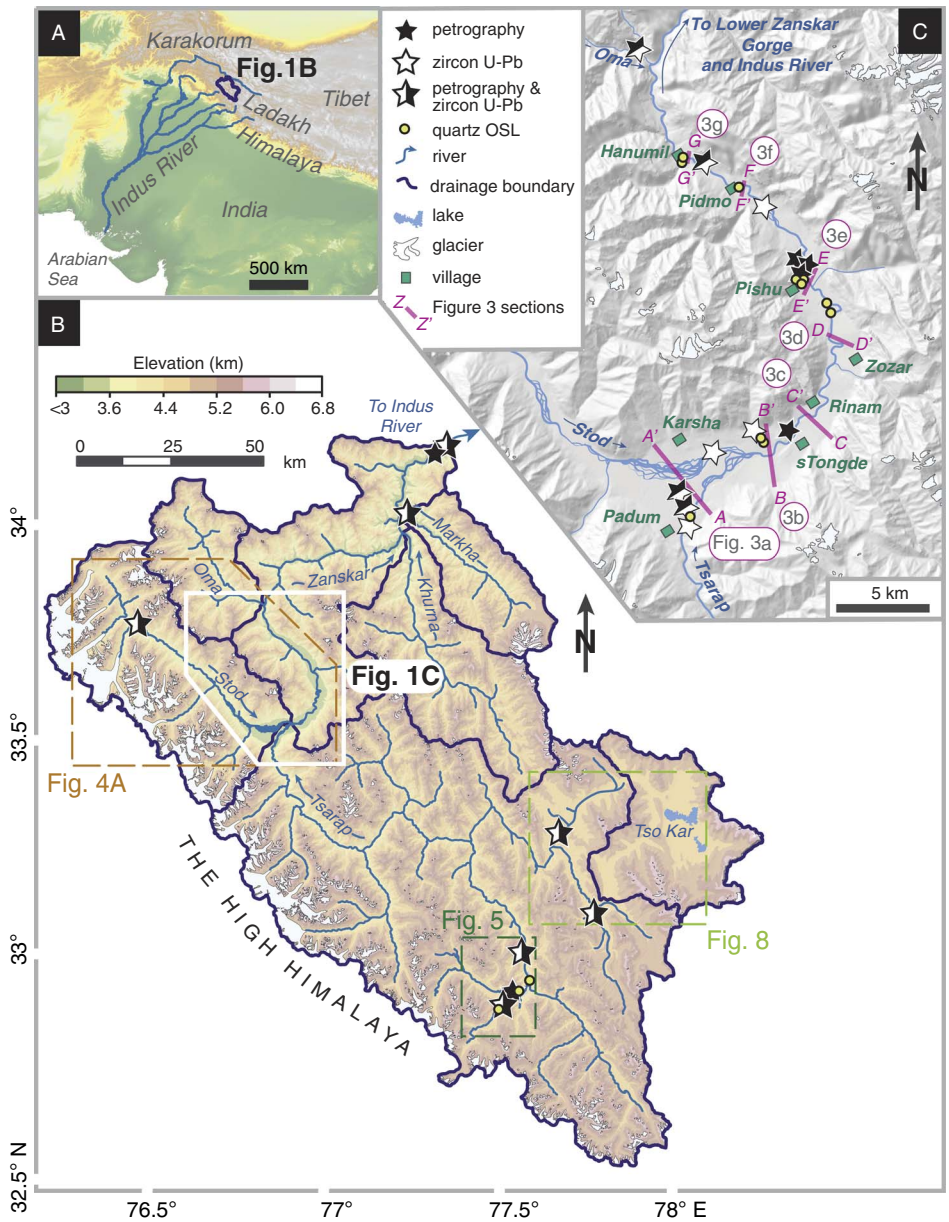

Figure 1. Setting of the Zanskar River relative to South Asia. (A) Location of Indus River (blue) and Zanskar River basin (black outline; Fig. 1B). (B) Topographic map river drainage and sample locations outside of the Padum basin. Dashed boxes indicate location of Figures 1C, 4, 5, and 8. (C) Digital elevation model map over the Padum basin indicating major tributaries (blue), sample locations (stars), and Figure 3 terrace section locations (pink lines). Topographic data are from Shuttle Radar Topography Mission 30 m grid data (SRTM30). OSL, optically stimulated luminescence. (For interpretation of the references to color in this figure legend, the reader is referred to the web version of this article.)

effects of transient storage and erosion of valley-fill sediments into the modern and Quaternary Indus River. Through optically stimulated luminescence (OSL) dating, sediment petrography, and detrital U-Pb zircon analysis, the ages and sources of valley-fill sediments are defined to help establish spatial patterns of erosion since ~35 ka. Estimates for volumes of stored valley-fill sediments are made from field observations and morphometric analysis. These findings are compared with regional sediment budgets to improve understanding of how, and over what time scales, climatic phases may influence sediment flux to the trunk Indus River through formation and erosion of Quaternary valley fills lying within the Himalayan rain shadow.

BACKGROUND

Sediment buffering in the Indus River

The Indus River system has routed water and sediment from the Tibetan Plateau and western Himalaya to the Arabian Sea for at least the last ~45 Ma (Clift et al., 2001). Four major Indus tributaries drain the Himalayan foreland basin, with the upper trunk of the Indus River cutting up through the northwest Himalaya and Karakoram onto the Tibetan Plateau (Fig. 1).

Modern erosion and sediment transport rates positively correlate with increased rainfall and discharge from the frontal Himalaya (Galy and France-Lanord, 2001; Gabet et al., 2008). Records from speleothems (Fleitmann et al., 2003), marine cores (Prins et al., 2000; Gupta et al., 2003; Staubwasser and Weiss, 2006), central Asian paleolake sediments (Fang, 1991; Gasse et al., 1991, 1996; Shi et al., 2001), and pollen records (Herzschuh, 2006) indicate strong Quaternary summer monsoon phases at ~44–34 ka and after the last glacial maximum (LGM; ~20 ka) to the mid-Holocene (~5 ka) across south and central Asia.

Summer monsoon intensity has critically controlled both the volumes and compositions of sediments delivered from the frontal Himalaya to the Indus delta and submarine fan, especially over the last ~20 ka. Strong shifts in bulk sediment Nd and Sr isotope geochemistry and detrital mineral provenance indicate increasing bedrock erosion along the frontal Himalaya synchronous with increasing monsoon rainfall intensity from 14 to 9 ka in Indus delta sediments (Clift et al., 2008). In addition, mid- to late Holocene downcutting of the Indus River into the alluvial plain began to significantly rework floodplain sediments into the Indus delta (Giosan et al., 2012). Until preindustrial damming of the Indus River, reworked valley-fill deposits were important to the overall delta sediment compositions (20–25% total mass flux), such that most other changes in upstream bedrock erosion and sediment provenance were strongly diluted (Clift and Giosan, 2014).

Dissected valley fills can be recognized even in the mountainous headwaters of the Indus River system across the Karakoram and Transhimalaya. Although some occur within steep bedrock gorges as a result of landslide and glacial damming (Hewitt, 1998, 2002; Dortch et al., 2010; Korup et al., 2010), alpine topography accommodates extensive alluvial sediments elsewhere in the northwest Himalaya. The longevity (~122–530 ka) of preserved valley-fill remnants attest to major cycles of Indus River aggradation and incision in the past (Blöthe et al., 2014; Munack et al., 2016). These deposits confirm long residence times and substantial erosion of sediments from the Indus headwater regions for at least the last two glacial cycles. Older moraine deposits (>385 ka; Owen et al., 2006; Blöthe et al., 2014) and abundant dammed lacustrine sediments, together with preserved undated terraces >400 m above modern river level (Pant et al., 2005; Phartiyal et al., 2005), further testify to at least >0.5 Ma history of sediment storage and residence in the upper Indus River basin.

Nevertheless, the degree to which erosion of Himalayan valley-fill deposits contributes to Quaternary upper Indus River sediment flux remains largely unresolved. Volumetric estimates, combined with cosmogenic-nuclide derived evidence, suggest erosion of valley fills may easily dominate over contributions from fresh bedrock erosion since the Pleistocene (Blöthe and Korup, 2013; Munack et al., 2016). Provenance studies, though just focused on the latest part of these time scales, do not indicate substantial erosion from Pleistocene terraces into the modern river bedload (Blöthe et al., 2014; Jonell et al., 2017) but also do not preclude valley-fill erosion having played a stronger role in the past under different climatic conditions and episodes of river incision. Although initial attempts to quantify buffering indicate rain shadow valley fills are not a dominant source in the Indus basin, these prior budgets were based on a number of assumptions and extrapolations that require age constraints and further validation from the field to establish their significance over wider areas of the Himalaya and over 10^3–10^4 yr time scales (Clift and Giosan, 2014).

Zanskar River climate and geology

This study investigates the Zanskar River, located in the Zanskar region of the Transhimalaya (Fig. 1). The modern Zanskar River basin can be divided into five subbasins of the main tributaries: the Tsarap, Stod, Khurna, Markha, and Oma. Adjacent to the Zanskar River basin is the internally drained Tso Kar basin (with an area of 1042 km^2). Lying north of the orographic barrier of the High Himalaya on the periphery of the Tibetan Plateau, the Zanskar River is characterized alternately by narrow bedrock gorges with rugged topography and peaks that rise to >6000 m above sea level (asl), as well as by broad (3–6 km), glacially modified river valleys ranging in altitude from ~3000 to 4500 m asl. Much of the Zanskar River basin has an alpine, desert-steppe rain shadow climate (Hartmann, 1987). A strong precipitation gradient is marked by higher mean annual precipitation (~400 mm/yr) along the backbone of the High Himalaya to only ~115 mm/yr in the Tso Kar basin (Bookhagen and Burbank, 2006). Precipitation is delivered in the summer months (June to August) by the Asian summer monsoon that pushes across the High Himalaya into the Tibetan Plateau. In

winter, snow is brought by the midlatitude winter westerlies (Benn and Owen, 1998).

In contrast to the Himalayan foreland, there is little consensus on the impact of monsoon precipitation on erosion in the Transhimalaya. Under modern, average monsoon conditions, summer rainfall in semiarid to arid catchments represents ~40% of the mean annual precipitation and contributes as little as 26% to the total discharge (Bookhagen and Burbank, 2010). Arid catchments receiving limited rainfall in the central Himalaya give commensurately low erosion rates (<0.1 mm/yr) in contrast to the summer monsoon–dominated catchments along the Himalayan front that yield rates of ~1–2 mm/yr (Gabet et al., 2008; Burbank et al., 2012). Some observations indicate monsoon storms trigger hillslope erosion producing a significant (30–50%) part of the annual suspended sediment flux in only a few events (Wulf et al., 2010, 2012). Similar flood impacts in the Ladakh Transhimalaya document discharges exceeding ~75–100% more than bankfull loads after intense summer storms (Hobley et al., 2012). Short-lived storm events, and potentially longer wetter monsoon phases, may critically control erosion from catchments that otherwise lack sufficient transport capacity under modern arid conditions (Bookhagen et al., 2005b; Hobley et al., 2012).

The bedrock geology of the Zanskar River basin (Fig. 2) can be grouped into three lithotectonic sequences: (1) the Greater Himalaya; (2) the Tethyan Himalaya; and (3) the Indus Suture Zone. The Greater Himalaya consists of Neoproterozoic-Ordovician paragneiss, metapelite, and orthogneiss (Honegger et al., 1982; Pognante et al., 1990; Spring et al., 1993; Noble and Searle, 1995; Horton and Leech, 2013; Horton et al., 2015). These rocks are largely considered to be the deeply buried, high-grade equivalents of the Tethyan Himalaya sequence, the former passive margin of Greater India.

Neoproterozoic to early Paleocene carbonate and siliciclastic sedimentary rocks comprise the very low- to low-grade

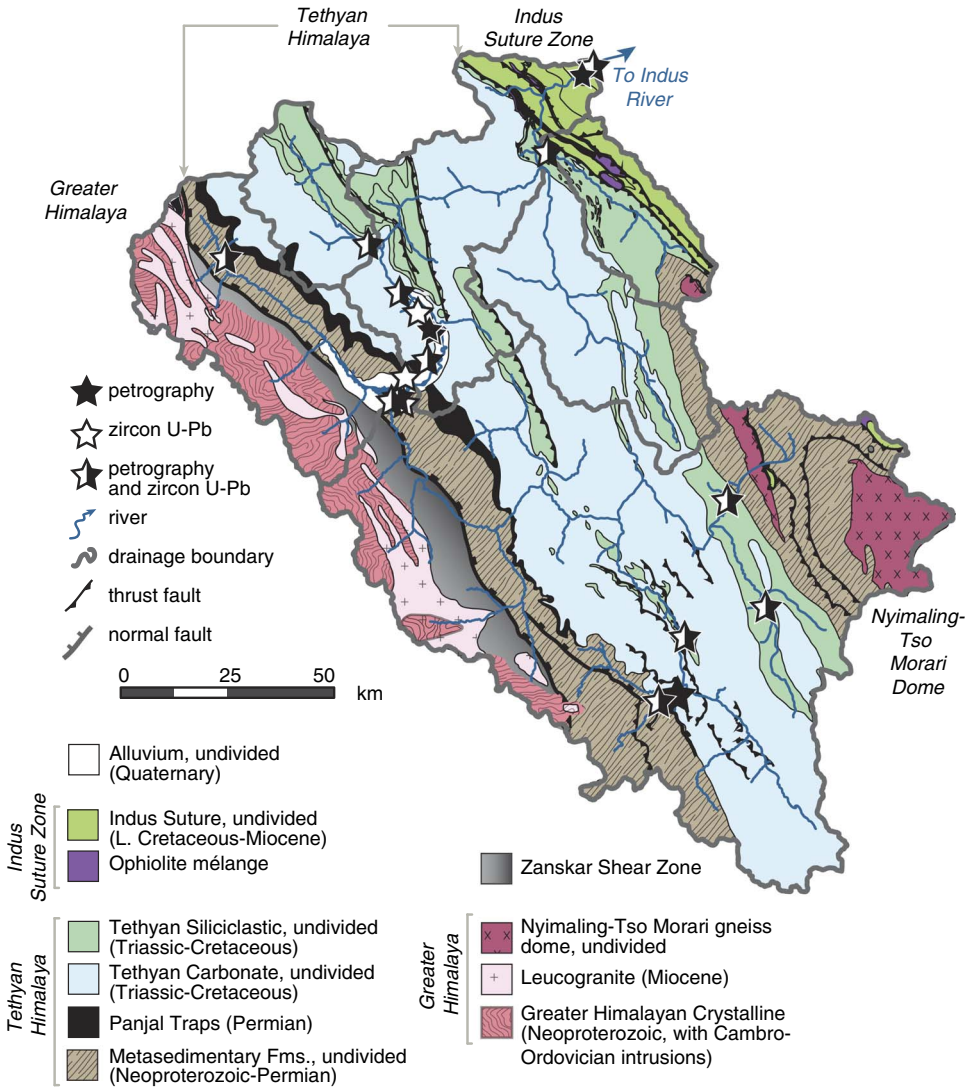

Figure 2. (color online) Simplified geologic map of the Zanskar River basin after Fuchs (1986), Fuchs (1987) with additions from Dèzes et al. (1999), southern Zanskar (Lahul) from Steck et al. (1993), and Tso Kar area (Epard and Steck, 2008). Sample locations denoted by stars. Modified after Jonell et al. (2017).

metasedimentary Tethyan Himalaya. Locally, Tethyan rocks reach lower amphibolite facies adjacent to the Nyimaling-Tso Morari dome and along the Zanskar Shear Zone, the ~150-km-long segment of the South Tibetan Detachment fault segregating the Greater and Tethyan Himalaya (Herren, 1987; Steck, 1993; Dèzes et al., 1999). Paleozoic magmatic pulses produced two suites of igneous rocks in the Zanskar River basin: (1) Pan-Africa Orogeny Cambro-Ordovician (550–440 Ma) granitic plutons (Cawood et al., 2007; Horton and Leech, 2013) and (2) Gondwanan rifting Panjal Traps flood basalts (~289 Ma) and associated Mississippian-Permian (380–245 Ma) granitic plutons (Shellnutt et al., 2012, 2014). Rocks of the third lithotectonic sequence, the Indus Suture Zone, record sedimentation related to Cretaceous-Eocene subduction and collision of Greater India and Eurasia (e.g., Searle, 1983; Searle et al., 1990). Ophiolitic mélange, Indus Molasse sandstones, and Cretaceous-Eocene forearc basin strata are exposed along the easternmost part of the basin (Clift et al., 2002; Henderson et al., 2010). This basin and the surrounding region have been relatively tectonically quiescent from the early to mid-Miocene (Schlup et al., 2003; Kirstein et al., 2006, 2009; Schlup et al., 2011) with no significant neotectonic activity recorded since that time (Jade et al., 2010).

Contemporary glaciers remain strictly confined to north-facing headwalls within the Zanskar basin (Benn and Owen, 1998; Dortch et al., 2011; Kamp et al., 2011; Owen and Dortch, 2014), but the many broad, overdeepened intermontane valleys of the region indicate extensive past glaciation (Owen et al., 2006; Korup et al., 2010; Bolch et al., 2012; Blöthe and Korup, 2013; Scherler et al., 2014). Glacial valley systems extended >50 km from present-day ice margins during the early last glacial period (Osmaston, 1994; Mitchell et al., 1999; Hedrick et al., 2011). Since that time, glaciers retreated regionally, with only small glacier advances confined <15 km from present-day ice margins in their respective catchments during the late glacial period (16–14 ka), Neoglacial period (4–2 ka), and Little Ice Age (~300–200 yr BP; Burbank and Fort, 1985; Owen, 2009; Owen and Dortch, 2014; Hedrick et al., 2017).

METHODS

To assess the provenance of river terrace sediments and constrain timing of sediment aggradation in the Zanskar River basin, field observations, sediment petrography, and detrital zircon U-Pb geochronology were integrated with OSL dating. The potential role of sediment buffering in the upper Indus River is assessed using morphometric analysis to identify regions hosting significant Quaternary sediments and calculate stored sediment volumes.

Field observations and sampling

All locations, elevations, and heights relative to the modern river level of Quaternary alluvial terraces were mapped over three field seasons from 2012 to 2014 using Landsat Enhanced Thematic Mapper Plus (ETM+) imagery from Google Earth (http://www.google.com/earth) and handheld Garmin ETrex GPS devices with an estimated vertical accuracy of ±2 m and horizontal accuracy ±10 m. Very fine to medium sands (>63 μm) were preferentially sampled from coarse sediment lenses in alluvial terrace stratigraphy (Figs. 3–5). The sand-size fraction is preferred for detrital mineral provenance analysis because this fraction does not place limits on laser ablation spot sizes that may decrease analytical accuracy. Sample locations are presented in Table 1 and given a number identifier for easier reference for the reader.

Sediment petrography

Unsieved, bulk terrace sediments were counted in thin section with at least 200 points following the Gazzi-Dickinson method (Ingersoll et al., 1984). All lithic fragments were classified by composition and in reference to the Metamorphic Index (MI) (Garzanti and Vezzoli, 2003; Vermeesch et al., 2016). Grain mounts were stained with alizarin red-S to distinguish calcite from dolomite. Sediments were classified according to the proportion of the main fragments (Q, quartz; F, feldspars; L, lithic fragments) and named by abundance when exceeding10% QFL point counts (e.g., litho-feldspatho-quartzose sand, Q > F > L > 10% QFL).

Environmental bias and intrasample variability as a result of hydrodynamic sorting processes were in part corrected for by applying a "source rock density" (SRD) correction to the bulk petrographic data. SRD corrections adjust the relative abundance of all lithic and mineral phases according to a specified bulk sediment density appropriate for sediment origin and degree of exhumation and erosion (Garzanti and Andò, 2007a, 2007b). Bulk petrographic data were corrected to an SRD value of 2.71 g/cm^3, considered appropriate for regions of the Himalayan orogen exposing Tethyan and Greater Himalayan strata. Bulk petrographic data are reported in Table 2 and shown in Supplementary Figure 1.

U-Pb zircon geochronology

Detrital zircon is a chemically and mechanically durable mineral phase in siliciclastic sediments such that multiple cycles of erosion do not significantly alter U-Th-Pb isotopic compositions (Gehrels, 2014). U-Pb dating of zircon has become an affordable, common tool for constraining sediment provenance, and a chronological database exists for reference on rivers draining the Himalayan-Tibetan orogen (Amidon et al., 2005; Alizai et al., 2011; Nie et al., 2015). Here, the 63–250 μm size fraction is analyzed because this fraction yields all significant U-Pb age populations present in detrital sedimentary samples (Yang et al., 2012). The application of U-Pb zircon dating to Zanskar River terrace sediments is in part enabled from similar analysis of modern Zanskar sediments with this technique (Jonell et al., 2017).

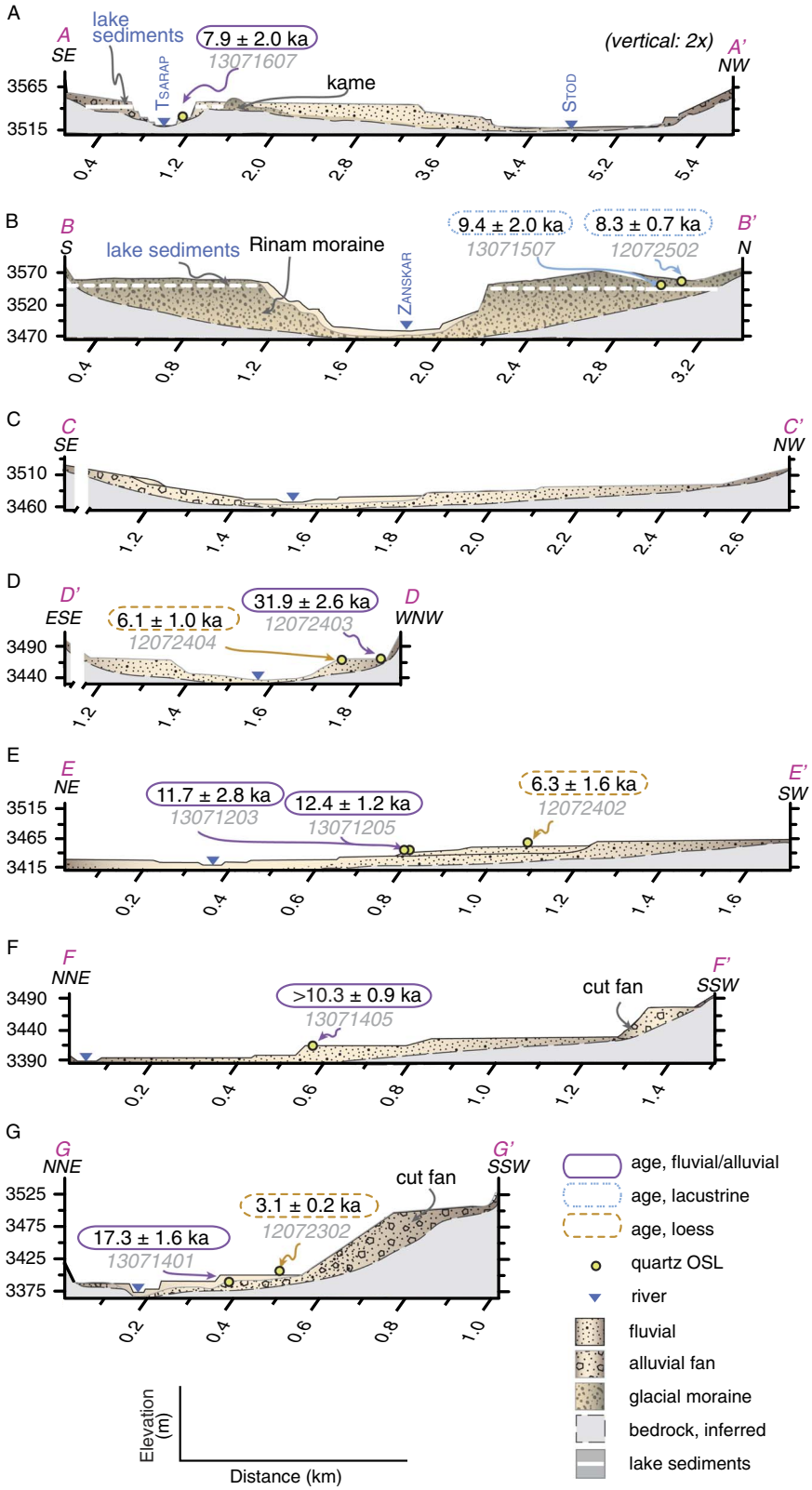

Figure 3. (color online) Schematic cross sections (A–G) of river terraces in the Padum basin. Section locations indicated in Figure 1C. OSL, optically stimulated luminescence.

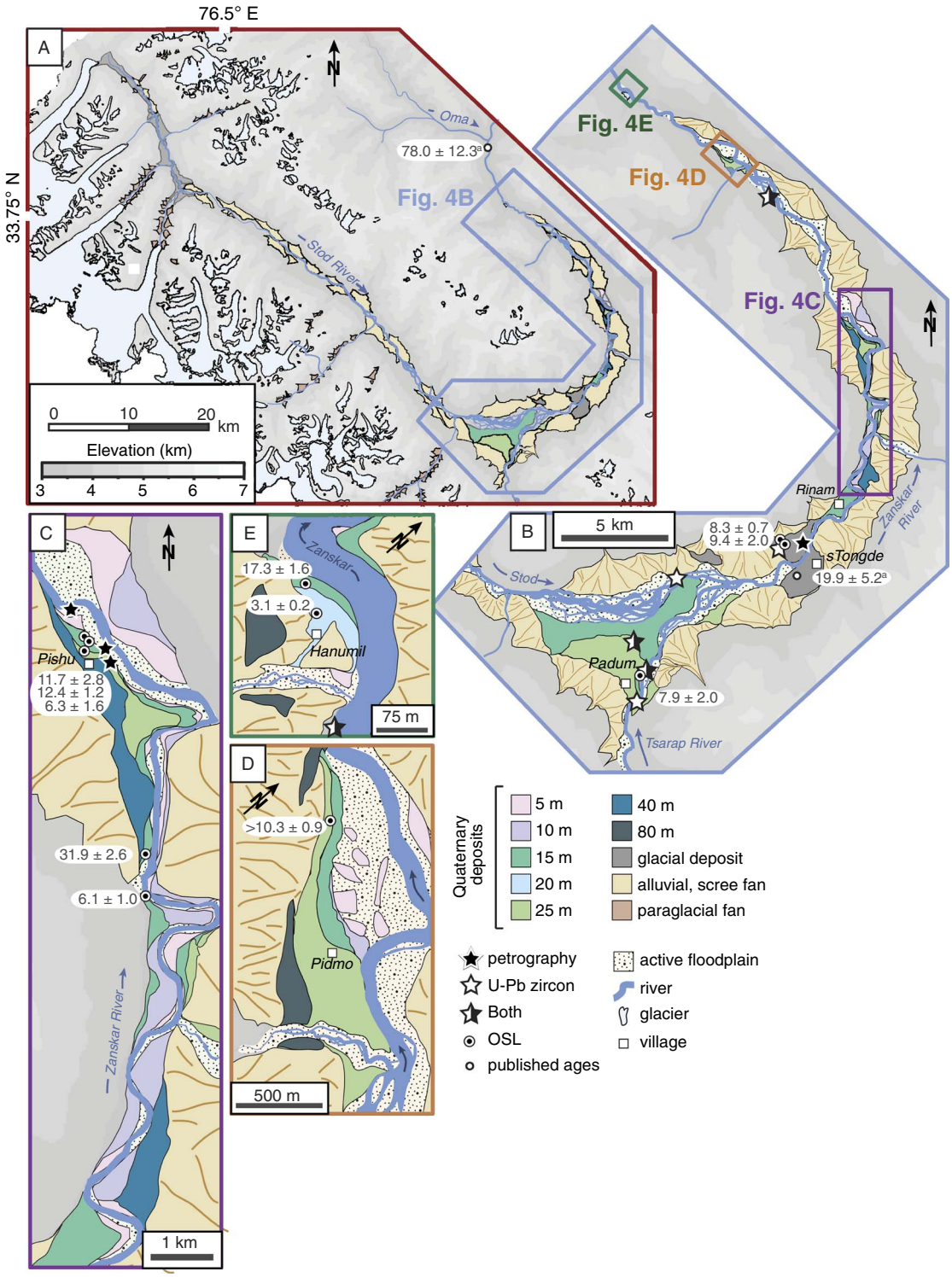

Figure 4. Geomorphological map of western Zanskar and Padum basin. (A) Quaternary deposits of Padum Basin and Stod River valley. (B) Quaternary deposits of Padum basin on trunk Zanskar River (blue lines). Boxes indicate locations of panels C–E. (C) Quaternary deposits at Pishu village. (D) Quaternary deposits at Pidmo village. (E) Quaternary deposits at Hanumil. Reported ages are from this study and Taylor and Mitchell (2000), denoted with (a). OSL, optically stimulated luminescence. (For interpretation of the references to color in this figure legend, the reader is referred to the web version of this article.)

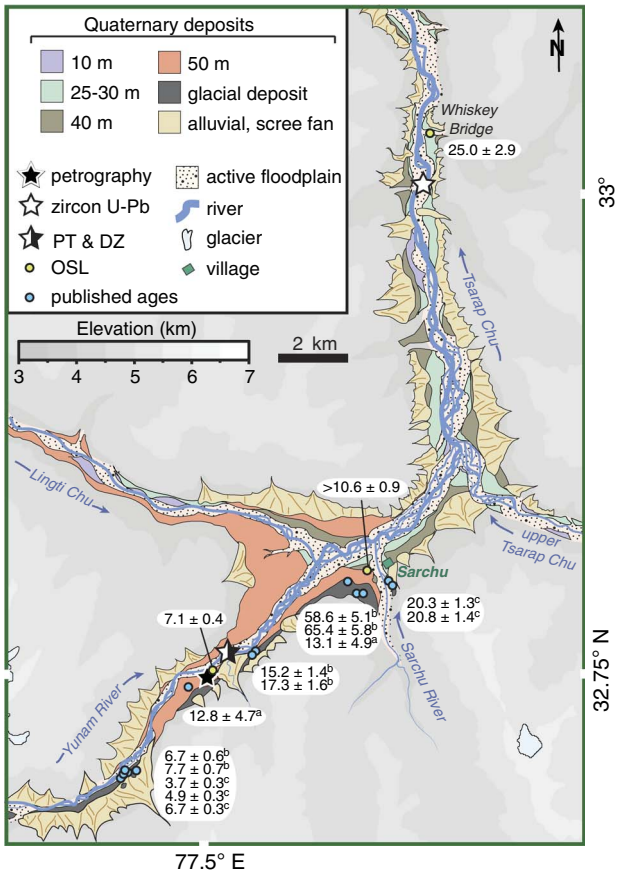

Figure 5. Geomorphological map of the eastern Zanskar River basin and Sarchu basin of upper Tsarap River (blue lines). Reported ages from this study and the following literature: (a) Taylor and Mitchell (2000); (b) Saha et al. (2016); and (c) Sharma et al. (2016). DZ, detrital zircon; OSL, optically stimulated luminescence; PT, sediment petrography. (For interpretation of the references to color in this figure legend, the reader is referred to the web version of this article.)

Detrital zircon grains were separated using standard magnetic and heavy liquid separation techniques. Extremely magnetic material was removed using a rare earth element hand magnet prior to sieving to 63–250 µm. Zircon grains were mounted in epoxy, polished, and imaged.

U-Th-Pb isotopic compositions were determined at the London Geochronology Centre facilities at University College London using a New Wave 193 nm aperture-imaged frequency-quintupled laser ablation system, coupled to an Agilent 7700 quadrupole-based inductively coupled plasma mass spectrometer. An energy density of ~2.5 J/cm^2 and a repetition rate of 10 Hz were used during laser operation. Laser spot diameter was ~30 µm with sampling depth of ~5 µm. Sample-standard bracketing by measurement of external zircon standard Plešovice (Sláma et al., 2008) and National Institute of Standards and Technology 612 silicate glass (Sláma et al., 2008) were used to correct for instrumental mass bias and depth-dependent intraelement fractionation of Pb, Th, and U. Temora (Black et al., 2003) and 91500 (Wiedenbeck et al., 2004) were used as secondary zircon age standards. Over 100 grains were analyzed for each sample to provide a statistically robust data set for lithologically diverse units (Vermeesch, 2004). Age data were filtered using a +5 and −15% discordance cutoff. For grains with ages less than 1000 Ma, the $^{206}Pb/^{238}U$ ratio was used, and the $^{207}Pb/^{206}Pb$ ratio for grains older than 1000 Ma. Data were processed using GLITTER 4.4 data reduction software (Griffin et al., 2008). Time-resolved signals recording isotopic ratios with depth in each crystal enabled filtering to remove signatures owing to mixing from overgrowth boundaries, inclusions, and/or fractures. Individual U-Pb ages are reported at 1σ. Analytical data and individual U-Pb ages are presented in Supplementary Table 1.

Detrital zircon U-Pb age data are presented in kernel density estimation (KDE) plots in the text for visual analysis of age population distributions and abundance (Fig. 6). KDE plots are favored in this study to prevent visual bias as traditional probability density functions may smooth older age populations with inherently larger age errors than younger populations at 1σ (Vermeesch, 2012). To quantitatively compare the intersample variability and compare age distributions with bedrock ages from the literature, the robust statistical multidimensional scaling (MDS) technique is applied using the open source 'provenance' package for R by Vermeesch et al. (2016). MDS analysis produces bivariate maps clustering samples presented here and against bedrock data compiled from literature based on Kolmogorov-Smirnov test dissimilarity (Figs. S2 and S3).

OSL dating

To define the timing of terrace aggradation and the relative timing of terrace abandonment and fluvial incision, sediments were dated using OSL. For this investigation, sediments likely bearing 63–150 µm quartz grains were sampled because quartz is a commonly targeted mineral in luminescence dating techniques. Furthermore, the 63–150 µm size fraction is the most readily transported and deposited in a fluvial setting (e.g., Rhodes, 2011). Samples were selected from sediment facies that are inferred to have received maximum light exposure during transportation, such as shallow channel sediments, to maximize bleaching and minimize inherited signals (Schaetzl and Forman, 2008). OSL samples were collected in ~15-cm-long aluminum tubes after cleaning surfaces of ~10 cm of material before sampling. All tubes were packed and wrapped with newspaper and UV-resistant tape, and double-bagged in opaque media for transport. OSL samples were processed and analyzed at the luminescence dating laboratories at the University of Cincinnati and the University of Oxford.

Quartz grains were isolated from heavy minerals and feldspars using pretreatment with HCl, HF, and fluorosilicic acids before heavy liquid separation and wet sieving. Modified single-aliquot regeneration (SAR) protocols (Wintle and Murray, 2006) were employed on small aliquots (200–500 grains; 100–150 µm in diameter) to estimate equivalent doses

Table 1. Sample locations for Zanskar River sediments. DZ, detrital zircon; OSL, optically stimulated luminescence; PT, sediment petrography.

ID	Sample	Location	Type	Latitude (°N)	Longitude (°E)	Elevation (m asl)	PT	DZ	OSL
1	8081203	Zanskar-Indus	Modern	34.162	77.326	3129	x	x	
1b	14072906	Chotski 20	Terrace	34.164	77.332	3143	x		
1c	10073101	Chotski 20	Terrace	34.164	77.332	3143			x
2	14072807	Markha	Modern	33.992	77.241	3311	x	x	
3	12072207	Oma Chu	Modern	33.792	76.829	3420	x	x	
4	13071402	Hanumil	Modern	33.716	76.877	3407	x	x	
4b	12072302	Hanumil (L)	Terrace	33.721	76.869	3390			x
4c	13071401	Hanumil	Terrace	33.720	76.867	3411			x
4d	13071405	Pidmo 25	Terrace	33.700	76.913	3421			x
5	12072401	Pishu	Modern	33.682	76.941	3411	x	x	
5b	12072403	Pishu	Terrace/fan	33.600	76.995	3500			x
6	13071201	Pishu	Modern	33.635	76.983	3433	x		
6b	12072402	Pishu (L)	Terrace	33.630	76.982	3460			x
6c	12072404	Pishu (L)	Terrace	33.595	76.996	3458			x
6d	12071203	Pishu 15	Terrace	33.632	76.984	3447			x
6e	13071205	Pishu 15	Terrace	33.632	76.984	3447			x
6f	13071503	Pishu 15	Terrace	33.629	76.992	3452	x		
6g	13071206	Pishu 25	Terrace	33.628	76.992	3466	x		
R1	13071507	Rinam Lake	Lake	33.535	76.954	3571			x
R2	13071504	Rinam 80	Terrace	33.531	76.966	3571	x		
R3	12072503	Rinam 80	Terrace	33.535	76.955	3571		x	
14	13071607	Padum 15	Terrace	33.478	76.892	3545			x
14b	13071609	Padum 15	Terrace	33.478	76.892	3545	x	x	
14c	13071602	Padum 25	Terrace	33.491	76.885	3553	x	x	
14d	12072501	Padum Lake	Lake	33.535	76.955	3577			x
7	12072504	Lower Stod	Modern	33.518	76.911	3520	x	x	
8	13071703	Upper Stod	Modern	33.817	76.432	4027	x	x	
9	12072507	Lower Tsarap	Modern	33.461	76.883	3540	x	x	
10	14080401	Zara	Modern	33.342	77.713	4454	x	x	
11	13072301	Toze Lungpa	Modern	33.124	77.774	4496	x	x	
12	13072302	Gata	Modern	33.008	77.594	4185	x	x	
13	14080609	Yunam	Modern	32.885	77.533	4328	x	x	
13b	14080602	Yunam 50	Terrace	32.880	77.530	4381	x		
13c	14080601	Yunam 50	Terrace	32.880	77.530	4381			x
S	13072304	Sarchu 15	Terrace	32.910	77.579	4311			x
W	12072902	Whiskey Bridge	Fan	33.024	77.592	4196			x

and establish signal growth curves. Ultrasmall aliquot (5–10 grains) quartz grain dating (Duller, 2008) was undertaken if partial bleaching yielding skewed equivalent dose distributions was noted. This allowed age calculations even where populations of grains of various bleaching ages were present (Bailey and Arnold, 2006; Jaiswal et al., 2008; Srivastava et al., 2008). Risø measurement systems were used to calculate paleodoses and dose response curves using a minimum of five SAR cycles under subdued sodium lighting (588 nm). Errors were estimated either with Monte Carlo simulation (2000 repeats) or calculated analytically, based on the difference between the fitted curve and dose points. Analytical uncertainties for OSL ages range typically from 5% to 10%. Estimations of the contribution of cosmic dose rate accounted for geographic position, elevation, topographic shielding, snow cover and depth, burial depth, and water content (Prescott and Hutton, 1994).

Field observations noted many prominent cut-and-fill aggradational terrace levels in two glacially modified basins at Padum and Sarchu (Figs. 3–5). Prominent terrace surfaces in each region were targeted because it was impractical to sample all terrace levels for dating. OSL age analyses are presented in Table 3. Field photographs outlining OSL sample locations and stratigraphy are included as Supplementary File 1.

Basin morphology and sediment volumes

Digital elevation model (DEM) topographic data were derived from void-filled 30 m grid Shuttle Radar Topography Mission (SRTM30) data. Modern glacial extents are from Global Land Ice Measurements from Space (GLIMS) Version 1 data (Bajracharya et al., 2014). River profile analysis was conducted using ArcGIS and TopoToolbox 2.0

Table 2. Bulk petrography of Zanskar River terrace sediments.

			Framework grains						Mica		Dense minerals									
ID	Sample	Location	Q	F	Lc	Lsm	Lm	Lv	Mu	B	ZTR	Ep	Gt	Ky	Sil	A	Px	Ap	&	Classification[a]	Dominant lithology
1b	14072906	Choksti 20	18	15	7	85	26	6	2	6	3	1	0	0	5	1	0	0	0	Quartzolithic	(Meta)carbonaticlastic
14c	13071602	Padum 25	14	20	19	105	33	3	1	2	0	0	0	0	1	0	0	0	0	Feldspatholithic	Metamorphiclastic
14b	13071609	Padum 15	6	11	72	76	25	0	2	2	1	0	1	0	1	1	0	0	0	Lithic	Metamorphiclastic
R2	13071504	Rinam 80	55	48	3	23	43	3	1	4	3	2	0	0	6	5	0	0	0	Feldspatho-quartzolithic	Metamorphiclastic
6g	13071206	Pishu 25	26	51	26	41	27	7	0	6	0	1	0	1	2	4	0	0	0	Quartzo-feldspatholithic	Carbonaticlastic
6f	13071503	Pishu 15	18	26	37	39	38	14	1	5	0	0	3	0	5	2	0	0	0	Quartzo-feldspatholithic	Metamorphiclastic
13b	14080602	Yunam 50	22	12	0	49	65	0	3	12	0	0	0	0	1	1	0	0	0	Quartzolithic	Metamorphiclastic

Notes: &, andalusite, staurolite, chloritoid, olivine, spinel, and monazite; A, amphibole; Ap, apatite; B, biotite; Ep, epidote; F, all feldspar; Gt, garnet; Ky, kyanite; Lc, all carbonate excluding metacarbonate; Lm, all higher rank (3-5) metamorphic fragments; Lsm, all sedimentary and low rank (1-2) metasedimentary terrigenous fragments after Garzanti and Vezzoli (2003); Lv, all volcanic fragments; Mu, muscovite; Px, pyroxene; Q, all quartz; Sil, sillimanite; ZTR, zircon, tourmaline, and rutile.
[a]Classified according to relative proportion of quartz (Q), feldspar (F), and lithic (L) material exceeding 10% of QFL total.

for MATLAB (Schwanghart and Scherler, 2014). Longitudinal river profiles were extracted for all major tributaries (draining more than 500 km^2) and for smaller tributaries containing significant valley fills using a carve-and-fill hydrologic conditioning routine. To identify locations and approximate thicknesses of valley fills along each longitudinal profile, swath profiles were extracted orthogonally along each channel every 500 m. Swath widths extended to within 2 km of significant valley fills or to 1 km if hillslopes were ≥20º (Fig. 7).

Table 4 summarizes volumes of sediments stored as Quaternary alluvial terraces, alluvial and paraglacial fans, and dissected glacial till in the Zanskar River and Tso Kar basins. Alluvial and paraglacial fan volumes were calculated individually for each feature after extracting landform geometries from Landsat ETM+ imagery and SRTM30 data. Fan volumes were determined using the fan apex to toe distance, apex and toe elevations, and fan toe circumference to calculate flat-based semicone volumes similar to the method of Giles (2010). Total fan volume estimates are assigned ±12% uncertainties reflecting that although fans are reasonably well defined, there are errors from measurement and simplified geometry that must be taken into account. Terrace volumes and dissected glacial till calculations followed a similar methodology to that of Clift and Giosan (2014) that considered terrace volumes as triangular sediment wedges. Subplanar terrace treads were identified by low slope (<2°) areas and terrace risers as edges with hillslopes ~2–8°. Terrace thicknesses were measured manually from the DEM after identification. Measured terrace thicknesses were no deeper than modern river level or exposed adjacent bedrock and assumed subparallel surface treads and bases. Terrace thickness calculations were balanced by stratigraphic observations made in the field. Uncertainties for terrace volumes are no more than 28% after taking into account propagated errors from terrace height and areal measurements. Sediment volumes for hillslopes, periglacial deposits, and noneroded glacial valley sediments were not calculated because cover thickness and bedrock depth were unknown. This results in our budget representing a robust, albeit likely minimum, estimate for stored sediment volumes. Exported sediment volumes were calculated as trapezoidal sediment wedges using the cross-sectional area of removed material across the river channel and the length of the deposit along the longitudinal river profile. We account for minor errors in measurement of removed material along river, deposit thickness, and width and assign a propagated uncertainty of no more than ±8% on exported sediment volumes. Field photographs of the major basins and valley fills are included in Supplementary File 2.

RESULTS

Sediment petrography

Zanskar River terrace sediments contain a diverse assemblage of mineral and lithic fragments (Table 2). Framework

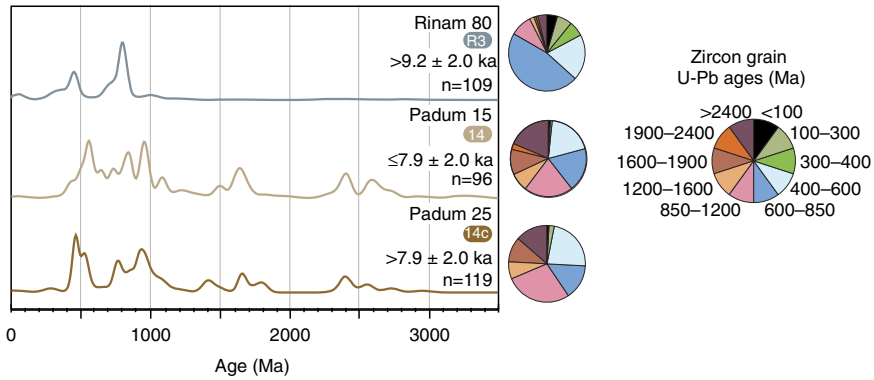

Figure 6. (color online) Kernel density estimation diagrams of detrital zircon U-Pb ages from Zanskar River terrace sediments with age interval ranges illustrated in pie diagrams.

petrography indicates abundant quartz, feldspar, low-rank metasedimentary and metacarbonate fragments, and high-rank fibrolite-bearing metafelsite fragments. Minor but notable fragments include serpentinized ultramafic and vesicular, porphyritic metabasite fragments. Abundant mineral phases include calcite and dolomite spar, micas, fibrolitic sillimanite, green and green-brown amphibole with minor garnet, zircon, and titanite. Bulk sediment compositions range from quartzolithic (meta-) carbonaticlastic to lithic metamorphiclastic.

Most terrace sediments approximately match rock compositions associated with Tethyan Himalaya provenance on a quartz-feldspar-lithic diagram (Supplementary Fig. 1). Exceptions to this are the eroded Rinam moraine (Table 1, ID #R2) and ~25 m Pishu terrace (ID #6g) samples that are more similar to Greater Himalayan sources. This in part is the result of the abundance of carbonate detritus in other sediments and slight enrichment in quartz and/or feldspar fragments, respectively, in Rinam and Pishu (Table 2).

U-Pb zircon geochronology

Detrital zircon spectra of the three terrace samples are presented as KDE diagrams following Vermeesch (2004) in Figure 6. The ~15 m Padum terrace (ID #14) sample is characterized by minor Archean ages as old as ~3800 Ma; small Proterozoic populations at 2600–2400 Ma, 1650 Ma, and ~1500 Ma; and a broad, composite peak of zircon ages from ~1100 to 450 Ma. Within the composite peak are subsidiary peaks at ~950, ~850, ~750, 600–500 Ma (545 Ma peak), and ~450 Ma. One Miocene zircon yielded an age of 22.1 ± 0.6 Ma. U-Pb zircon ages from ~25 m Padum terrace (ID #14c) yielded similar, prominent strong age peaks at ~750, ~530, and ~450 Ma, with smaller populations at 2600–2400, ~1800–1600, and ~1400 Ma. Younger zircons include one Miocene zircon at 25 ± 0.9 Ma and two Permo-Triassic zircons at 281 ± 7 and 251 ± 7 Ma. The Rinam moraine sample (ID #R3) contains peaks at ~545, ~440, and 380–245 Ma, with a very strong peak at 850–650 Ma. This sample yielded the most Miocene zircon (n = 5) with ages ranging from 26 to 21 Ma.

OSL dating

Eleven new OSL samples were dated from the Padum basin (Figs. 3 and 4; Supplementary File 1). The confluence of the Stod and Tsarap Rivers near Padum village hosts two prominent terrace surfaces at 25–30 m and 10–15 m above modern river level (Figs. 3A and 4B). An OSL age from a coarse silt ~0.5 m below the top of the ~15 m terrace surface yielded an age of 7.9 ± 2.0 ka. Downriver from the Stod-Tsarap confluence, 2–3 m of laminated lacustrine sediments overlie an incised 80- to 90-m-thick terminal moraine. Laminated silts ~1 m from the base of the section yielded an age of 8.3 ± 0.7 ka (Figs. 3B and 4B). A fine laminated silt at the base of the section overlying poorly sorted, pebbly silt till was dated to 9.4 ± 2.7 ka. Similar but less thick (~1 m) lacustrine sediments occurring at the same elevation are discontinuously exposed ~8 km upstream of the Rinam moraine at Padum village (Figs. 3A and 4A).

Several incised terrace surfaces were dated downstream of the Stod-Tsarap confluence near Padum village. Near Pishu village, a prominent ~40 m terrace composed of poorly sorted, matrix-supported sandy cobble conglomerate yielded an age of 31.9 ± 2.6 ka from an interbedded ~0.2-m-thick medium sand lens (Figs. 3C and 4C). This ~40 m surface extends ~12 km upstream to Rinam village and discontinuously ~8 km downstream to Pidmo village (Figs. 3D and 4D). A discontinuous, thin (~0.5 m) loess cap occasionally exposed on top of the ~40 m terrace surface was dated to 6.1 ± 1.0 ka at Pidmo village (Fig. 3D). At Pishu village, a similar thin loess cap (<0.5 m thick) overlying a ~25 m terrace surface yielded an age of 6.3 ± 1.6 ka (Figs. 3E and 4C). The ~25 m terrace surface extends downstream ~8 km to Pidmo village and is often preserved adjacent to the ~40 m terrace surface (Fig. 4C). An OSL age of 10.3 ± 0.9 ka was obtained from the top of the ~25 m terrace from a medium silt layer located ~1.5 m below a 0.5-m-thick silty-clay soil horizon at Pidmo village (Figs. 3F and 4D). At Pishu village, a very fine sand below a ~15 m terrace surface was dated beneath a 0.3-m-thick silty-clay soil horizon dated at 11.7 ± 2.8 and 12.4 ± 1.2 ka (Figs. 3E and 4C).

Terraces remnants are preserved as far downstream as Hanumil village in the Padum basin (Figs. 3G and 4E).

Table 3. Optically stimulated luminescence sample results.

Field sample	Laboratory name	Location	Elevation (m)	Elevation above river (m)	Depth (m)	Particle size (μm)	In situ H_2O (%)[d]	U (ppm)	Th (ppm)	K (%)	Rb (ppm)	Cosmic (Gy/ka)[e]	Dose rate (Gy/ka)	Number of aliquots[f]	Equivalent dose, D_e (Gy)[g]	OSL age (ka, ±1σ)[h]
10073101	Chotski	Chotski 20[a]	3143	18	4.8	212–250	0.09	1.95	8.79	0.99	–	0.30 ± 0.15	2.02 ± 0.09	5	7.71 ± 3.65	3.8 ± 1.8
12072302	X6003	Hanumil (L)[c]	3390	15	<1	180–255	6.22	3.90	16.40	1.82	96.0	0.31 ± 0.03	3.86 ± 0.13	9	12.11 ± 0.73	3.1 ± 0.2
13071401	X6354	Hanumil[c]	3400	25	1	180–255	0.33	2.50	11.40	1.36	76.0	0.32 ± 0.03	2.89 ± 0.10	11	50.06 ± 4.29	17.3 ± 1.6
13071405	Pidmo Sand	Pidmo 25[b]	3421	25	1.5	90–150	0.42	2.80	12.10	1.16	60.0	0.35 ± 0.04	2.92 ± 0.14	6	29.11 ± 2.31	10.3 ± 0.9[i]
12072402	X6001	Pishu (L)[c]	3460	40	1.5	180–255	8.93	3.10	10.00	1.70	61.0	0.28 ± 0.03	3.05 ± 0.10	10	19.14 ± 4.96	6.3 ± 1.6
12072403	UIC3322	Pishu 25[b]	3500	40	3	100–150	0.97	3.70	16.50	1.71	–	0.29 ± 0.03	3.87 ± 0.17	17	123.64 ± 7.70	31.9 ± 2.6
12072404	X6002	Pishu (L)[c]	3458	25	1.5	180–255	5.43	2.70	12.00	1.11	55.0	0.28 ± 0.03	2.67 ± 0.09	11	16.30 ± 2.53	6.1 ± 1.0
13071203	Pishu	Pishu 15[b]	3447	15	1.8	90–150	–	3.40	15.30	1.25	66.0	0.34 ± 0.04	3.37 ± 0.17	24	38.04 ± 7.93	11.7 ± 2.8
13071205	X6351	Pishu 15[c]	3447	15	1.2	180–255	4.50	3.10	16.90	1.81	59.0	0.31 ± 0.03	3.75 ± 0.12	9	46.54 ± 4.40	12.4 ± 1.2
13071507	Rinam Lake	Rinam Lake[b]	3571	81	1.5	90–150	0.63	3.60	18.10	1.34	61.0	0.35 ± 0.04	3.70 ± 0.19	23	38.04 ± 7.76	9.4 ± 2.0
13071607	L-Podum	Padum 15[b]	3545	10	0.5	90–150	3.32	2.5	10.90	1.23	65.0	0.35 ± 0.04	2.84 ± 0.03	21	22.26 ± 5.59	7.9 ± 2.0
12072501	X6000	Rinam Lake[c]	3577	89	0.9	180–255	0.20	4.30	22.30	1.12	52.0	0.29 ± 0.03	3.77 ± 0.12	9	31.24 ± 2.44	8.3 ± 0.7
12072902	12072902	Whiskey Bridge[c]	4196	26	3	180–255	14.73	2.50	12.30	1.37	70.0	0.31 ± 0.03	3.05 ± 0.10	10	66.15 ± 7.49	25.0 ± 2.9
13072304	L-Sorchu	Sarchu[b]	4311	14	0.5	90–150	0.07	1.80	8.10	0.84	42.0	0.35 ± 0.04	2.12 ± 0.10	8	27.8 ± 0.93	10.6 ± 0.9[i]
14080601	14080601	Yunam 50[c]	4381	50	1.3	180–255	0.33	2.40	13.20	1.44	75.0	0.47 ± 0.05	3.13 ± 0.15	11	22.63 ± 1.21	7.1 ± 0.4

[a]Department of Geography, Royal Holloway, University of London.
[b]Luminescence Dating Lab, Department of Geology, University of Cincinnati.
[c]Research Laboratory for Archaeology and the History of Art, University of Oxford.
[d]Assume 5 ± 2 wt% H_2O is representative of burial history.
[e]Contribution of cosmic radiation to the dose rate was calculated by using sample depth, elevation, and longitude/latitude following Prescott and Hutton (1994).
[f]Number of aliquots used for age calculation. Rejection of aliquots follows standard rejection criteria
[g]D_e calculated using the minimum age model of Galbraith et al. (1999) unless otherwise noted; Excel macros written by Sébastien Huot (UQAM). Université du Québec à Montréal (UQAM).
[h]Uncertainty on age is 2-sigma standard error.
[i]Minimum age because of low intensity.

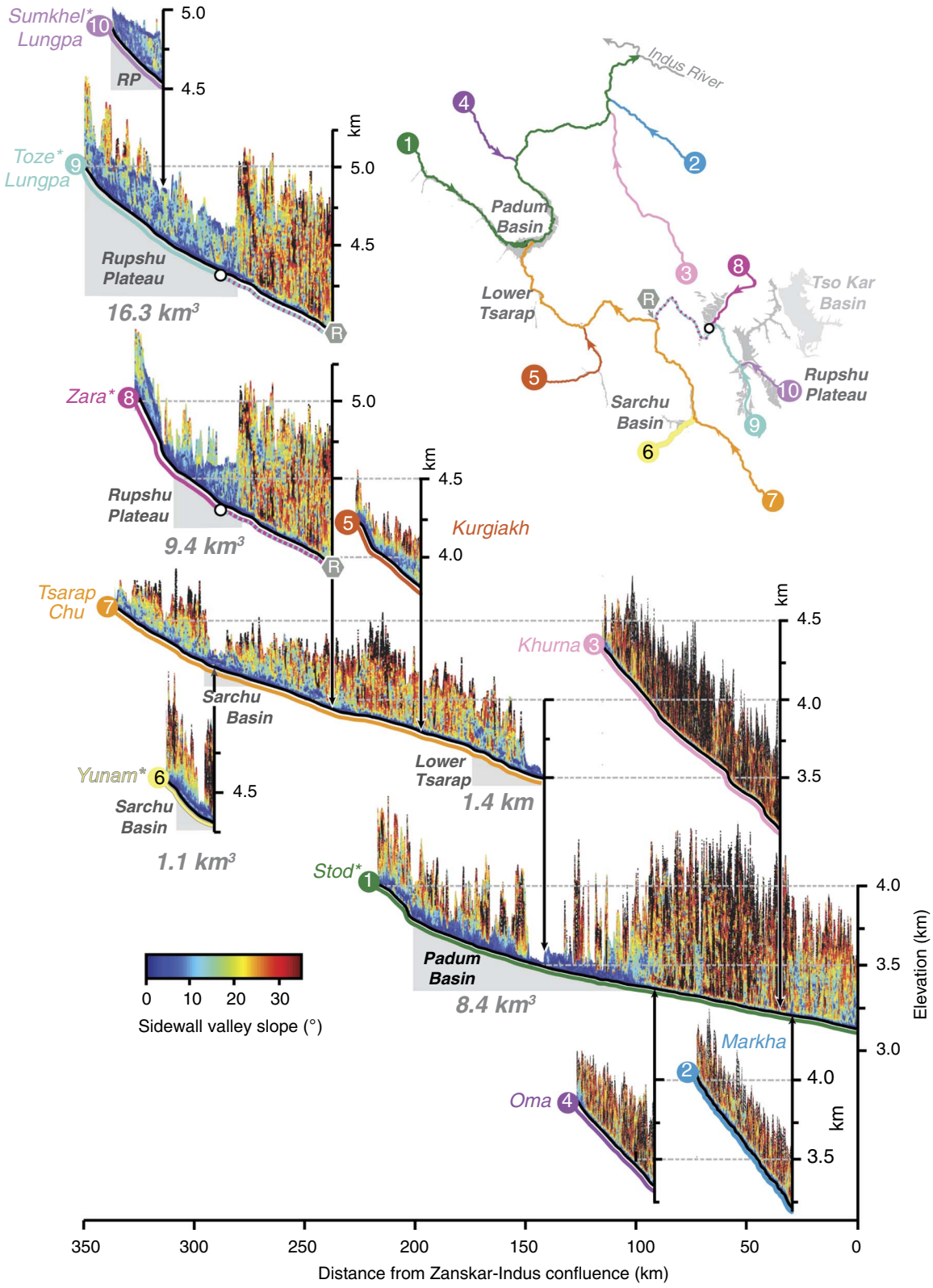

Figure 7. Stacked elevation-slope channel profiles of the Zanskar River and locations of large valley-fill deposits. Slope values (<35°) were extracted along the river channel every 500 m orthogonal to the channel to confining bedrock hillslopes. Swath width was 2 km from river channel except rivers with bedrock confining hillslopes within 1 km of channel indicated by asterisks (*). Lower slope values (<10°, blue) are layered above higher slope values to indicate regions of sediment storage. To best illustrate the extent of Rupshu Plateau valley fills from Munack et al. (2016), the Toze Lungpa and Zara River profiles overlap. Gray shaded regions on longitudinal profiles and within the inset indicate large valley fills in the Padum basin, lower Tsarap, Sarchu basin, Rupshu Plateau, and Tso Kar basin. Sediment volumes reported in Table 4 are next to each valley fill. Tso Kar basin valley fill is shown in light gray. RP, Rupshu Plateau (includes the More Plain). (For interpretation of the references to color in this figure legend, the reader is referred to the web version of this article.)

Table 4. Stored sediment volumes for Zanskar River and Tso Kar basins.

Region	Stored volumes (km^3)	% Total stored	Area (km^2)	Area connected (km^2)	Accessible volume[a] (km^3)	% Total stored[a]
Padum basin						
Terraces	1.3 ± 0.4	4 ± 1.0	42 ± 4.1			
Glacial deposits	0.7 ± 0.2	2 ± 0.6	11 ± 1.0			
Fans	6.3 ± 0.8	17 ± 2.1	0.1 ± 0.01			
Basin subtotal	8.4 ± 1.3	23 ± 3.6	52.4 ± 5.1	52.4 ± 5.1	8.4 ± 1.3	55 ± 8.7
Lower Tsarap						
Glacial deposits	1.2 ± 0.3	3 ± 0.9	7 ± 1.1			
Fans	0.3 ± 0.04	1 ± 0.1	<0.1 ± 0.0			
Basin subtotal	1.4 ± 0.4	4 ± 1.0	7.1 ± 1.1	7.1 ± 1.1	1.4 ± 0.4	9 ± 2.3
Sarchu basin						
Terraces	0.8 ± 0.2	2 ± 0.6	17 ± 2.6			
Fans	0.3 ± 0.03	1 ± 0.1	<< 0.1 ± 0.0			
Basin subtotal	1.1 ± 0.3	3 ± 0.7	17 ± 2.6	17 ± 2.6	1.1 ± 0.3	7 ± 1.7
Rupshu valley fill[b]						
More Plain	16.3 ± 4.6	44 ± 12.5	147 ± 22.0	26 ± 3.9		
Zara	9.4 ± 2.6	26 ± 7.2	61 ± 9.1	11 ± 1.6		
Basin subtotal	25.7 ± 7.7	70 ± 21.1	208 ± 31.1	37 ± 5.5	4.4 ± 1.2	29 ± 7.8
Total Zanskar (this study)	36.7 ± 9.7	–	–	–	15.3 ± 3.2	–
Tso Kar (this study)[c]	6–31	–	124	0	0	0
Blöthe and Korup (2013)						
Padum basin	12.0					
Sarchu basin	0.7					
Rupshu valley fill[d]	20.0					
Subtotal	32.7					

[a]Volumes within 500 m buffer zone on each side of river drainage.
[b]More Plain surface dated by Munack et al. (2016).
[c]Tso Kar valley fill depth ranging 50–250 m.
[d]Includes More Plain and Tso Kar only.

An age of 17.3 ± 1.6 ka was yielded from an interbedded fine sand between poorly sorted, pebble-supported sand at Hanumil village. A thin (<0.5 m) loess deposit found capping a 15–20 m terrace surface was also dated to 3.1 ± 0.2 ka.

Extensive dissected alluvial fans and river terraces are found within the Sarchu basin (Fig. 5). A ~60-m-thick incised alluvial fan was dated near Whiskey Bridge. A coarse sand lens within poorly sorted sandy conglomerate yielded an age of 25.0 ± 2.9 ka. A prominent terrace surface ~12–15 m above the modern river was dated near Sarchu village. A thin (0.25 m) medium sand lens interbedded in cobble conglomerate yielded a minimum age of 10.6 ± 3.6 ka. One of the most prominent terrace surfaces in the Sarchu basin, a ~50-m-thick valley fill composed of alternating coarse sand, imbricated fluvial pebbles, and poorly sorted sandy conglomerate alluvial fan lenses, extends several kilometers along the Yunam River and Lingti Chu tributaries. A medium sand layer below a ~1-m-thick poorly sorted pebbly sand yielded an age of 7.1 ± 0.4 ka.

Upstream of the Zanskar River–Indus River confluence at Choksti, one OSL sample from a ~20 m alluvial terrace perched on a bedrock strath terrace (Fig. 1B) yielded an age of 3.8 ± 1.8 ka.

Basin morphology and sediment volumes

There are four regions storing significant sediment volumes in the Zanskar River basin: the Padum and Sarchu basins, the Rupshu Plateau, and the lower Tsarap River (Table 4; Fig. 7). The Padum basin, which here includes all sediments in the Stod River catchment, and from the Stod-Tsarap confluence downstream to Hanumil village, is estimated to hold 8.4 ± 1.3 km^3 of sediment, predominantly as alluvial and paraglacial fans (Fig. 4). Latest Pleistocene–earliest Holocene river terraces account for only 1.3 ± 0.4 km^3 of sediment. In the Sarchu basin, 1.1 ± 0.3 km^3 of sediment is divided among Pleistocene-Holocene terraces and mixed alluvial/scree fans. The greatest volumes of sediment in the Zanskar River basin are stored as dissected valley fills that include the ~135 ka Rupshu Plateau outlined by Munack et al. (2016). Rupshu Plateau Pleistocene valley fills account for 25.7 ± 7.7 km^3 of sediment held as 110- to 150-m-thick valley fills in the Zara River catchment, and 90- to 240-m-thick valley fills held in the Toze Lunpga and Sumkhel Lungpa catchments (Fig. 8). We further estimate storage of sediment in the Tso Kar basin. Sediment volumes range from 6 to 31 km^3 depending on the

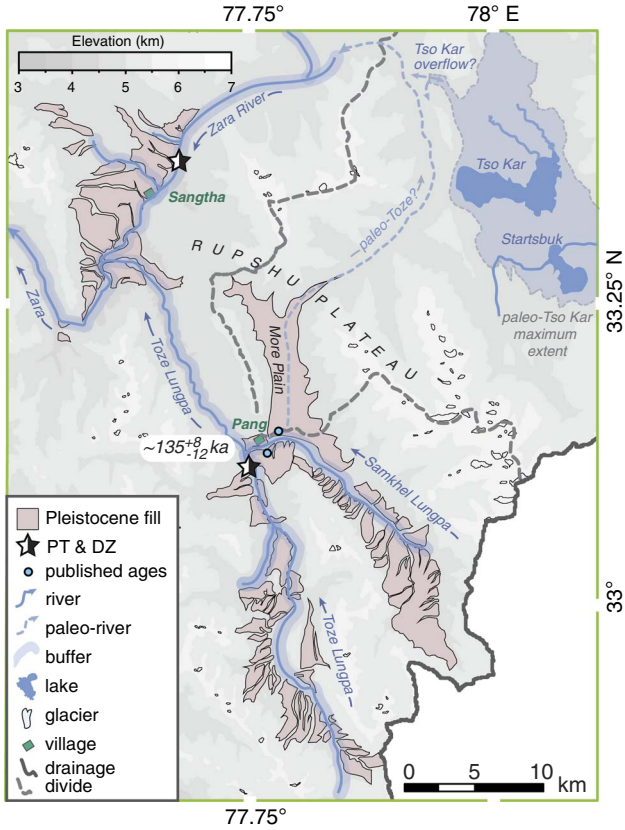

Figure 8. Pleistocene Rupshu Plateau valley fills (pink) of the More Plain and upper Tsarap River tributaries, the Toze Lungpa, Sumkhel Lungpa, and Zara River (blue lines). Tso Kar maximum extent (shaded blue) after Wünnemann et al. (2010). Proposed paleo-Toze Lungpa drainage (dashed blue) and reported in situ ^{10}Be exposure ages of ~135 ka for the Rupshu Plateau from the More Plain (Munack et al., 2016). DZ, detrital zircon; PT, sediment petrography. (For interpretation of the references to color in this figure legend, the reader is referred to the web version of this article.)

estimated valley-fill thickness (50–250 m) and a valley-fill area of ~124 km^2. Dissected moraines and paraglacial fans in the lower Tsarap catchment host 1.4 ± 0.4 km^3 of sediment.

DISCUSSION

Quaternary sediment provenance

Spatial patterns of erosion can be constructed through time by tracking the compositional evolution of both modern river and dated terrace sediments downstream (Fig. 9). Data presented here are compared with similar analyses from modern Zanskar River sediments (Jonell et al., 2017) to elucidate how paleo–Zanskar River compositions evolved locally downstream. We further evaluate if incision of stored valley fills may have been influential to the overall net export of sediments to the Indus River.

The Stod River has been previously proposed as the most significant source of sediment to the Zanskar River because of the abundance of Greater Himalayan lithic fragments, quartz and feldspar fragments, and abundant detrital zircon with peak ages of 850–750, ~450, and ~350 Ma for sediment from the modern river (Jonell et al., 2017). Downstream of the Stod River–Tsarap River confluence to form the trunk Zanskar River, sediments vary little until the trunk river enters the Zanskar Gorge (Fig. 9). Sediments evolve downstream to include more sedimentary and low-rank metasedimentary fragments from Tethyan Himalayan exposed along the bedrock gorge. If all tributaries are scaled to upstream contributing area, the greatest apparent contributor of sediment to the trunk Zanskar River is the Tsarap River catchment (Fig. 9A). Petrographic and detrital zircon data indicate that it is the smaller, slightly wetter, and glaciated Stod River catchment that has strongly moderated downstream sediment compositions with material from the Greater Himalaya not only under modern environmental conditions as suggested by Jonell et al. (2017), but consistently over the Holocene.

New data from Quaternary deposits suggest that erosion and recycling of Rinam moraine sediments along the trunk Zanskar River may also in part strongly control downstream sediment compositions for at least the last 12 ka. MDS analysis of bulk sediment point counts from the Rinam moraine (ID #R2) indicate closest similarity in provenance to the modern lower Stod (ID #7) and Zara (ID #10) River samples because of similar abundance of quartz and feldspar fragments (Fig. 10A). MDS analysis discretely groups Rinam moraine detrital zircon (ID #R2) with the modern Zanskar-Indus confluence (ID #1), Hanumil (ID #4), Pishu (ID #5), upper Stod (ID #8), and lower Stod (ID #7; Fig. 10B) sediments that all contain prominent age peaks mentioned previously (Supplementary Fig. 3).

It is most likely that Rinam moraine sediments were deposited from a valley glacier originating from the Stod River valley, eroding Zanskar Greater Himalaya rocks (Fig. 10C; Supplementary Fig. 2). Provenance data support this model because all significant zircon U-Pb age populations in the Zanskar Greater Himalaya are also identified in detrital zircon yielded from the Rinam moraine. Furthermore, Rinam yields high-grade lithic and fibrolitic sillimanite fragments associated with Greater Himalayan rocks within and outside the Zanskar River basin. Although MDS analysis of petrographic data (Fig. 10A) suggests the Zara River (ID #10) as a potential source, this is only a product of the coarse quartz and feldspar grains found in both the Rinam moraine and Zara River samples (Fig. 9; Table 2).

OSL ages in the Padum basin can be used to establish limits on glacial extent along the trunk Zanskar River, as well as the age of the Rinam moraine. Terrace age data require that the valley glacier system extended no farther than Hanumil village after ~17.4 ka and retreated past Pishu village by ~12 ka and to past Padum village by ~7.9 ka (Fig. 4). Many Padum basin incised alluvial fans ~40–80 m above the modern river imply a much earlier retreat. If an alluvial fan dated at ~32 ka (Table 3, sample 12072403) is considered representative of alluvial fan sedimentation in the basin, then the river may have been glacier-free downstream of Pishu village before the LGM. These data follow along with previous findings from Taylor and Mitchell (2000) arguing for a glacial maximum extent beyond Hanumil village from ~78 ka until at least 40 ka and a

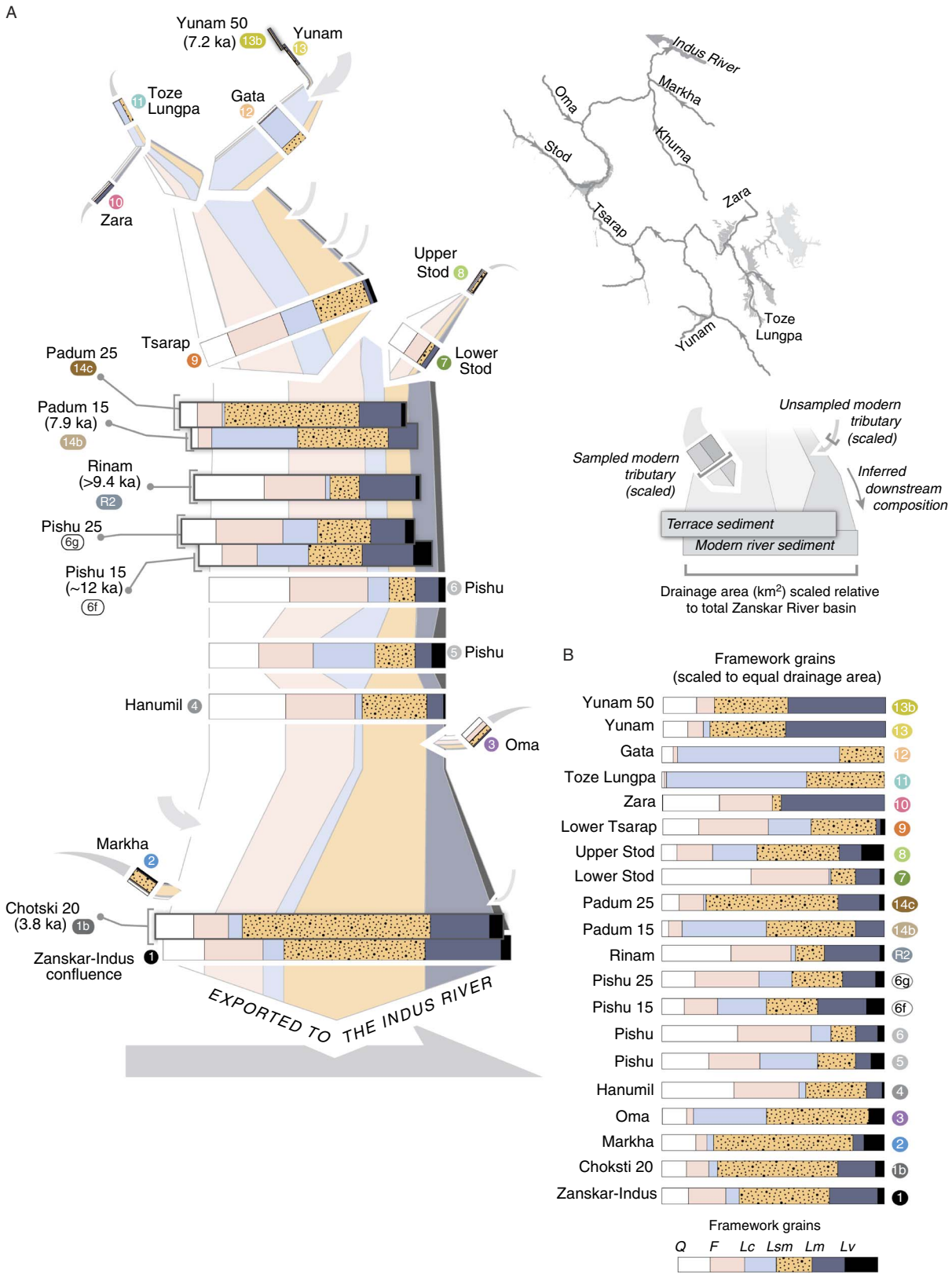

Figure 9. (color online) Bulk petrography of framework grains from selected terrace sediments and modern river tributary sediments (Jonell et al., 2017). (A) Downstream mixing schematic of river and terrace sediments from the trunk Zanskar River and major tributaries. Bars are proportionally scaled to the upstream contributing drainage area relative to the area of the Zanskar River basin (14,939 km^2). (B) Comparison of all sediment samples assuming equal upstream contributing drainage area. F, feldspars; Lc, lithic carbonate; Lm, medium- to high-rank metamorphic; Lsm, other sedimentary and low-rank metasedimentary; Lv, volcanic and metavolcanic; Q, quartz. Framework categories follow Garzanti and Vezzoli (2003). Samples are labeled and numbered after Table 1.

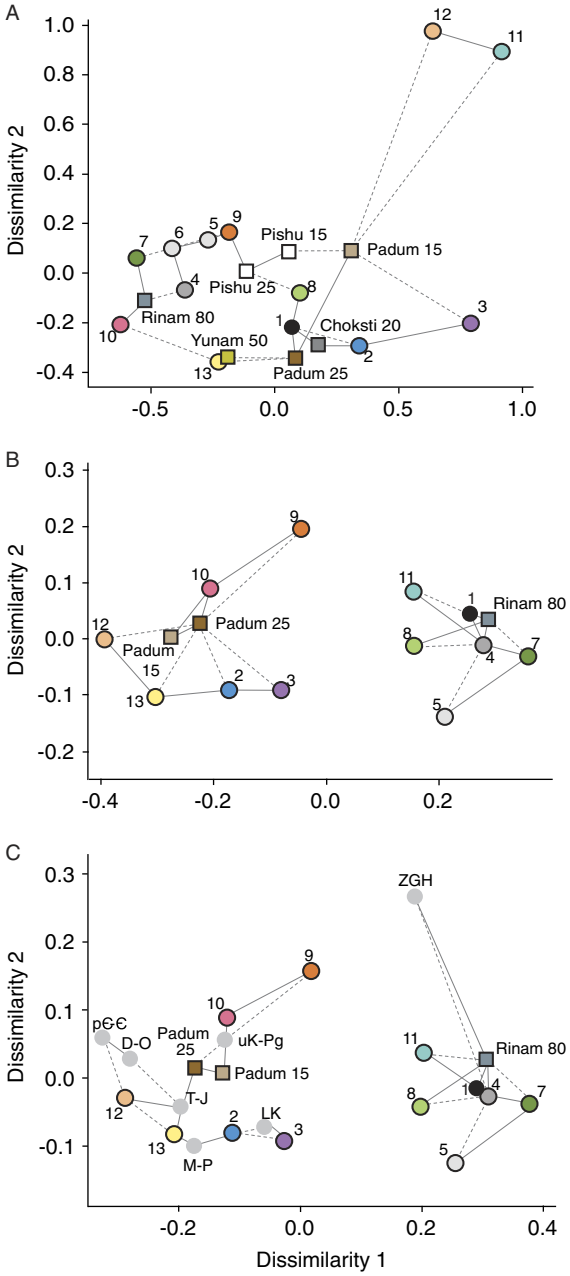

Figure 10. Multidimensional scaling (MDS) plots showing the Kolmogorov-Smirnov distances between modern Zanskar River sediments (color circles), river terrace sediments (squares), and local bedrock (gray circles). Number labels follow Table 1. (A) Nonmetric MDS plot of source rock density–corrected bulk petrographic data. (B) Nonmetric MDS plot of all Zanskar River detrital zircon U-Pb ages. (C) Zanskar River terrace sediments compared with modern Zanskar River sediments and compiled regional Himalayan bedrock U-Pb zircon ages (Figs. S1 and S2). Solid lines indicate closest neighbor and dashed lines nearest next neighbors. Data plotted using R 'provenance' package by Vermeesch et al. (2016). Bedrock abbreviations mostly follow depositional ages: D-O, Devonian to Ordovician; LK, lower Cretaceous; M-P, Mississippian to Permian; pЄ-Є, Proterozoic to Cambrian; T-J, Triassic to Jurassic; uK-Pg, upper Cretaceous to Paleogene; ZGH, Zanskar Greater Himalayan bedrock (Horton and Leech, 2013). (For interpretation of the references to color in this figure legend, the reader is referred to the web version of this article.)

subsequent retreat to Rinam village by 19.9 ± 5.5 ka. Our data generally agree with the chronology of Taylor and Mitchell (2000), although the accuracy of these earlier OSL ages has been called into question (Owen et al., 2002).

Similarly, time constraints on the incision of the Rinam moraine can be inferred. The age of the lake sediments dammed behind the Rinam moraine requires the moraine to be older than ~9.4 ka, with damming having occurred at least by that time (Figs. 3 and 4B). Moraine dissection must have occurred after lake sedimentation ended at ~8.2 ka, if not before upstream river incision through correlative lake sediments and Padum basin terrace aggradation at ~7.9 ka. If we consider that dissection occurred by ~7.9 ka, and if incision occurred over ~4.8 km of the river through the thickness of the moraine (80 m), an estimated 0.3 ± 0.03 km^3 of moraine material was transported into the Zanskar River downstream since that time. This volume equates to ~22% of the total stored sediment at present in the Padum basin (Table 4). If dissection of glacial valley-fill deposits held in the Stod River were also incised at that time, this would provide an additional 0.2 ± 0.02 km^3 of sediment.

Although erosion of valley-fill deposits significantly controls sediment compositions in the Padum basin, side valley contributions within the Zanskar Gorge moderate this effect downstream. Sediment compositions at the Zanskar River–Indus River confluence are not identical to those in the Padum basin (Figs. 9B and 10). This can be observed at least over the last ~3.8 ka as recorded at Choksti (ID #1b), suggesting that the bulk provenance of sediment fluxed from the Zanskar River to the trunk Indus has not changed significantly since at least that time.

Nonetheless, intrabasinal temporal provenance variations are recorded in terraces of fill-cut series in the Padum basin (Fig. 9B). First, a shift in provenance is noted between the ~25 m Pishu terrace (ID #6g) and the ~15 m Pishu terrace (ID #6f). Compositions at ~12 ka included more gneiss, calc-gneiss, fibrolitic sillimanite, and volcanic fragments than younger sediments (Table 2). This could suggest either increased erosion of Greater Himalayan and Panjal Traps bedrock exposed upstream along the Stod River and around Padum village or increased erosion of glaciofluvial outwash sediments derived earlier from Greater Himalayan and Panjal Traps bedrock. The relative contributions from fresh or reworked sediment cannot be determined using these new data, but we argue that erosion of valley fills is the most important sediment supply because deeply incised glaciofluvial gravels are observed throughout the Stod River valley (Fig. S2).

The provenance of terraces near Padum reflects a broad change in erosion patterns across the Tsarap River basin between 12 and ~7.9 ka. Between construction of the ~25 m (ID #14c) and ~15 m (ID #14b) Padum terraces, compositions evolved to include more Tethyan Himalayan lithologies (Figs. 9 and 10). Sediment compositions changed from predominantly high- and low-grade metamorphic fragments to include abundant carbonate, as also observed in the modern upper Tsarap River (ID #11, 12). Detrital zircon U-Pb ages also document a subtle shift by ~7.9 ka from populations similar to Triassic-Jurassic strata to populations found

more in upper Cretaceous and Paleogene siliciclastic strata (Fig. 10B and C). Together these data sets suggest a general shift from concentrated erosion of rocks exposed in the High Himalaya in the west and southwest of Zanskar to a broader erosional regime also tapping sediment sources in the eastern Zanskar River basin.

We infer that increasing influence of the summer monsoon and winter westerlies drove enhanced erosion and produced this marked intrabasinal shift in sediment provenance by ~7.9 ka. Before deposition of the ~15 m Padum terrace by ~7.9 ka, erosion was concentrated predominantly in regions exposing Greater Himalaya and Neoproterozoic to Jurassic Tethyan Himalaya (Fig. 2). This is similar to modern-day conditions where precipitation and erosion are focused along the High Himalaya (Jonell et al., 2017). By 7.9 ka, increased yield from rocks exposed in the eastern Zanskar River implies increased erosion of Tethyan Himalaya bedrock and/or large-scale erosion of voluminous Rupshu Plateau sediments held in the upper Tsarap River catchment. Net incision of Padum basin terraces must have occurred by ~6.2 ka (Fig. 3). Loess deposits preserved on some Padum terrace levels definitively mark abandonment of Padum basin terraces by that time. A second loess cap at Hanumil indicates abandonment and incision of terrace surfaces there at the latest by 3.1 ka (Fig. 4).

At least one phase of Pleistocene alluvial fan sedimentation and one phase of aggradation can be defined in the Sarchu basin (Fig. 5). Alluvial fan sedimentation at Whiskey Bridge was active until at least 25.6 ka. Aggradation of glaciofluvial outwash gravels in the Sarchu basin began before ~10.6 ka. The low intensity of induced luminescence during OSL dating underscores that this is a minimum age, and therefore, valley infilling must have initiated earlier. Sharma et al. (2016) suggest much earlier deposition over Marine Oxygen Isotope Stage 3 (~57–29 ka) for much of the Sarchu basin, where data here indicate either a second phase or a continuing phase of aggradation through ~7 ka as marked by the ~50 m terrace along the Yunam River (Table 3).

Incision within the Sarchu basin can be constrained in part using the recent glacial landform chronology of Saha et al. (2016). Glaciers extended no farther than Sarchu village as early as ~60 ka, then retreated to the middle Yunam River valley by ~16 ka and the upper Yunam River valley by ~7 ka. With these previous chronologies, a younger Holocene phase of net incision is established in the Sarchu basin after ~7 ka that worked to shape many of the prominent terraces surfaces ≤50 m in height.

Evacuated sediment from the Sarchu basin, in a similar fashion to the Padum basin, is predominantly sourced from glaciofluvial outwash rather than freshly eroded bedrock. The prominent ~50 m terrace shares similar petrography to the modern Yunam River (Figs. 9 and 10A). Both contain abundant gneiss, calc-gneiss, and foliated metapelite fragments from deformed, medium- to high-grade Neoproterozoic-Triassic rocks exposed upstream. We suggest a minimum of $0.5 \pm 0.06\,km^3$ has been eroded and exported from the ~50 m terrace along the Yunam River and adjacent Lingti Chu since terrace abandonment at early as ~7 ka.

Quaternary climate and sediment dynamics

The data presented here provide new constraints on Pleistocene and Holocene infilling and erosion that expand prior chronologies across the Zanskar River basin and other neighboring Transhimalayan basins (Dortch et al., 2011; Blöthe et al., 2014; Munack et al., 2016). From these findings, a late Pleistocene to Holocene sedimentation history can be constructed for the middle and upper Zanskar River basin (Fig. 11). Age constraints pinpoint at least two early phases of net aggradation and at least one younger net phase of incision: late Pleistocene alluvial fan sedimentation from at least ~32–25 ka with potentially concurrent deglacial aggradation; latest Pleistocene–earliest Holocene aggradation (~12–8 ka); and mid-Holocene net incision initiating by ~8–6 ka across the Zanskar River basin and continuing to the present. Near the Zanskar-Indus confluence, a small phase of late Holocene local aggradation at Choksti is recorded at ~3.8 ka with ~20 m of incision since that time.

Ages from bedrock and alluvial terraces along the Zanskar River Gorge and Zanskar-Indus confluence indicate major aggradation at ~50–20 ka, with two younger phases of net incision at 14–9.5 ka and prior to 6.3 ka (Dortch et al., 2011; Blöthe et al., 2014). Fluvial phases presented here from the middle and upper Zanskar River correspond with regional aggradation (~15–10 ka) and incision (<10–8 ka) in the frontal Himalaya that was previously shown to covary with monsoon strength (Pratt et al., 2002; Bookhagen et al., 2006; Srivastava et al., 2008; Thakur et al., 2014; Dey et al., 2016). Although temporal correlation between these two regions implies a common driver (i.e., summer monsoon intensity), glaciation and winter midlatitude westerlies strength also strongly control fluvial and sedimentation dynamics in the Transhimalaya (Demske et al., 2009; Wünnemann et al., 2010; Lee et al., 2014; Owen and Dortch, 2014; Mishra et al., 2015).

Hillslope processes operating at high elevation in semiarid regions, such as frost cracking and salt weathering, cannot be discounted as strong drivers of erosion in the Zanskar River basin (e.g., Bull and Knuepfer, 1987; Hales and Roering, 2005, 2007; Scherler et al., 2014). High-altitude hillslope processes are well recognized as primary generators of sediment along the Indus River valley and within the Rupshu Plateau (Blöthe et al., 2014; Dietsch et al., 2015; Munack et al., 2016). We argue that although hillslope processes are effective at generating sediment in high-elevation, arid regions within the Zanskar River basin, these processes are less influential than periglacial and fluvial processes in controlling the net export of sediments from the Zanskar River. The slower rates at which hillslope processes operate in the presently unglaciated catchments of Zanskar (i.e., the Rupshu Plateau) are not comparable to either the rates or volumes of sediments exported from the active, glaciated catchments.

Variations in the intensity of the summer monsoon and westerlies worked in concert with local glaciation to produce late Quaternary aggradation and incision, as recorded in

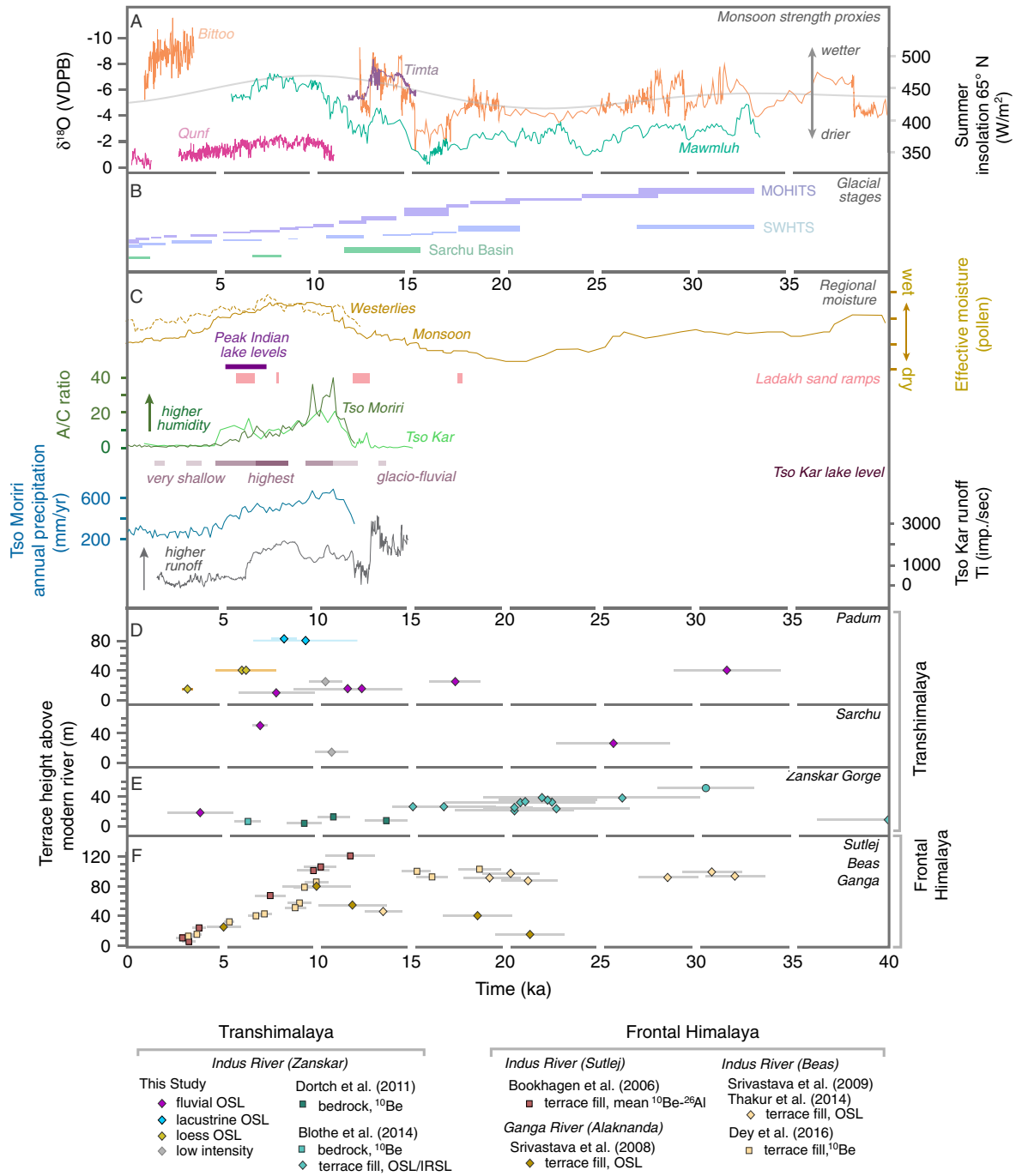

Figure 11. (color online) Selected Quaternary paleoclimate and paleoenvironmental proxies for South Asia. (A) Monsoon strength proxies compiled from cave records from Qunf, Oman (Fleitmann et al., 2003); Bittoo, India (Kathayat et al., 2016); Mawmluh, India (Dutt et al., 2015); and Timta, India (Sinha et al., 2005), with summer insolation for 65°N (Berger and Loutre, 1991). VPDB, Vienna Pee Dee belemnite. (B) Glacial stages for the northwestern Himalaya. Monsoonal Himalayan-Tibetan stages (MOHITS) after Murari et al. (2014), semiarid western Himalaya-Tibetan stages (SWHTS) after Dortch et al. (2013), and Sarchu basin from Saha et al. (2016). Bar heights indicate relative uncertainty for each stage. (C) Records for moisture transport from central Asian lake pollen records (Herzschuh, 2006), compiled lowland Indian lake levels (Clift and Plumb, 2008), eolian Ladakh sand ramps (Kumar et al., 2017), and pollen and paleohydrologic records from Tso Moriri (Leipe et al., 2014; Mishra et al., 2015) and Tso Kar (Demske et al., 2009; Wünnemann et al., 2010). (D) Optically stimulated luminescence (OSL) depositional ages of river terraces from the Zanskar River (this study). (E) ^{10}Be exposure ages and OSL/infrared-stimulated luminescence (IRSL) depositional ages of river terraces in the lower Zanskar Gorge (Dortch et al., 2011; Blöthe et al., 2014). (F) Select frontal Himalaya river terrace ages from the Sutlej (Bookhagen et al., 2006), Beas (Srivastava et al., 2009; Thakur et al., 2014; Dey et al., 2016), and Alaknanda Rivers (Srivastava et al., 2008). Cosmogenic nuclide ages for the Transhimalaya and frontal Himalaya were recalculated using CRONUS-Earth online calculators, Version 2.2. Error bars are 1σ.

the Zanskar River basin. Enhanced precipitation and rising temperatures associated with a strong monsoonal phase at 29–24 ka (Bookhagen et al., 2005a) coincided with local glacier retreat to further promote local aggradation and alluvial fan sedimentation (32–25 ka) along oversteepened Zanskar River valley walls (Sharma et al., 2016). This interval of increased moisture transport across the High Himalaya is recorded throughout the western Tibetan Plateau in lake sediments (Gasse et al., 1991, 1996; Shi et al., 2001), pollen records (Herzschuh, 2006), and river terraces (Dortch et al., 2011).

Later strengthening of the summer monsoon and westerlies into the early Holocene corresponded with increased erosion along the High Himalaya and aggradation in the Padum basin beginning ≥12 ka and ending at ~8 ka. This relationship with rainfall contrasts with work from glaciated mountain valleys in New Zealand where valley aggradation is associated with times of colder, drier climate (Bull and Knuepfer, 1987). This disparity likely reflects the fact that the New Zealand example receives much more annual precipitation (800–1200 mm/yr) in a glaciated maritime climate, with the highest basin elevations near but below modern treeline at ~1150 m. The Zanskar River, in contrast, receives as much as 450 mm to <100 mm/yr (basin average = 320 mm/yr) precipitation, with elevations between ~3100 and above 6000 m asl, and lies predominantly above the treeline in a cold desert-steppe climate. Expansion of strong precipitation during the Holocene climatic optimum further into the Himalayan rain shadow by ~8 ka triggered significant erosion of the Tethyan Himalaya bedrock as well as fluvial incision of the Rupshu Plateau valley fills. Early to mid-Holocene lake records document a very wet, warm interval from 11.8 to 7 ka at Tso Kar (Demske et al., 2009; Wünnemann et al., 2010) and at ~11–8 ka in Tso Morari (Leipe et al., 2014; Mishra et al., 2015). These data sets align with the model presented here, suggesting a shift from isolated erosion along the High Himalaya to broader, more regional erosion across the Zanskar River basin during the Holocene climatic optimum, as strong moist monsoonal and westerlies systems penetrated into the Tibetan Plateau for a prolonged time.

Subsequent weakening of the summer monsoon and westerlies led to decreased moisture transfer through the mid-Holocene that resulted in decreased river discharge, lower sediment flux by 7–6 ka, and net terrace incision on the northern side of the High Himalaya. Incision occurs because the rivers were carrying less sediment from the higher reaches and had excess carrying capacity that allowed them to erode into their former valley fills. With continued weakening of the summer monsoon and westerlies into the late Holocene, Tethyan Himalaya sediment flux waned. Basin-wide fluvial terrace incision and deposition of loess within Zanskar indicate a drying of the climate, consistent with several paleomonsoon climate records for that time (e.g., Prins et al., 2000; Fleitmann et al., 2003). Modern focused glacial erosion and precipitation along the west and southwest edge of the Zanskar River basin supports relatively higher Greater Himalayan sediment flux and continued incision of valley fills.

The sensitivity of the edge of the western Tibetan Plateau to climate-modulated buffering may directly reflect its location relative to the Himalaya rainfall maximum. The southwest edge of the Zanskar River basin lies ~100 km from the rainfall maximum, compared with >200 km to the Zanskar River–Indus River confluence and ~180 km to the Rupshu Plateau. The Zanskar River basin is not unique among Transhimalayan basins in containing large valley fills, but it may be that only marginal basins, including possibly the upper Sutlej River basin (i.e., Wulf et al., 2012), receive enough moisture to overcome thresholds for transport capacity that otherwise is extremely limited in high and dry Tibetan plateau interior basins (Dietsch et al., 2015). Such valleys are also subject to periglacial frost cracking when the moisture supply reaches a high enough level that in turn is known to be a very efficient mechanism for generating large sediment volumes (Walder and Hallet, 1985; Hales and Roering, 2005). Working together, these processes can drive significant sediment transport.

Quaternary buffering and sediment recycling

Quaternary valley fills account for $36.7 \pm 9.7\,km^3$ of stored material in the Zanskar River basin, with roughly 70% of this volume (~$26\,km^3$) held in the Rupshu Plateau (Fig. 8 and Table 4). The overall volumetric estimates presented here are strikingly consistent with previous valley-fill estimates ($32.7\,km^3$) using DEM algorithm-based extraction (Blöthe and Korup, 2013). Previous basin-specific estimates from Blöthe and Korup (2013) underestimate volumes in the Sarchu basin (~1.1 vs. $0.69\,km^3$) while overestimating volumes in the Padum basin (~8.4 vs. $11.9\,km^3$). These differences likely result from direct field evidence regulating calculations in this study, especially concerning valley-fill extent and depth. Nevertheless, the general agreement between these studies reinforces the general scale of the sediment budget and furthermore highlights the effectiveness of each technique in assessing sediment volumes over particular spatial scales.

Although the results discussed here indicate considerable sediment stored in the Zanskar River basin, not all of the stored sediment is readily erodible. Some valley-fill deposits may be relatively disconnected from the drainage network, such as sediments perched ~250–300 m above the entrenched rivers of the Rupshu Plateau. In that area, the older sediments are preserved in terraces that fill valleys that stretch far from the modern river channel. Because they receive little rainfall, there is minimal transfer of material from the terraces to the modern stream (Supplementary Fig. 2). This study attempts to account for this connectivity by using a 1-km-wide buffer around the drainage network to approximate how much sediment can be eroded into the river drainage through lateral incision, bank failure, and localized debris flows. This width is an arbitrary distance based on observations from modern incision patterns that can establish a conservative estimate. Volumes of erodible sediment adjust to $15.3 \pm 3.2\,km^3$ for the total Zanskar River. This is comparable to the estimates

Table 5. Zanskar River sediment yield estimates.

Basin	Basin area (km^2)	Mean volume (km^3)	Bulk density (g/cm^3)	Yield (10^6 t/km^2)	Average yield rate ($t/km^2/yr$) over: 10 ka	20 ka	135 ka
Total Zanskar River	14,939	36.7	1.9	4.7	467	233	35
Total Zanskar River[a]	14,939	15.3	1.9	2.0	198	99	15
Sediment <35 ka[a]	14,939	11.1	1.9	1.4	142	71	10
Sediment >35 ka[a,b]	14,939	4.4	1.9	0.6	56	28	4
Pre-Holocene Zanskar[c]	14,939	45–60	1.9	5.7–7.6	570–760	285–380	42–56
Total Export Zanskar[a,d]	14,939	23–38	1.9	3.6–4.9	361–488	181–244	27–36
Clift and Giosan (2014)							
Zanskar River	15,000	7–22	1.9	0.8–2.8	89–279	44–139	7–21
Munack et al. (2016)							
Rupshu Plateau[e]	773	11–19	1.9	27.8–46.0	2780–4604	1390–2302	206–341
Rupshu Plateau from Zanskar	14,939	11–19	1.9	1.4–2.4	144–238	72–119	11–18
Rupshu Plateau from Tsarap	7619	4.4	1.9	1.1	110	55	8

[a]Adjusted volumes for sediment connectivity.
[b]Sediment >35 ka is Rupshu Plateau valley fill.
[c]Stored (36.7 km^3) + eroded volumes (7–22 km^3) from Clift and Giosan (2014) and (11–19 km^3) Munack et al. (2016).
[d]Stored and connected (15.3 km^3) + eroded volumes (7–22 km^3) from Clift and Giosan (2014).
[e]More Plain, Toze Lungpa, Sumkhel Lungpa only.

for the total eroded sediment volumes over the last ~10 ka of 7–22 km^3 (Clift and Giosan, 2014), which were based on extrapolation of rates estimated from the trunk Indus River and are thus not very reliable. Further calculations indicate an additional ~4 km^3 of erodible sediment stored in the Rupshu Plateau. These corrected volumes imply that much of the Rupshu Plateau valley fill is relatively isolated from the modern Zanskar River system. Deep incision and excavation (11–19 km^3; Table 5) over the last ~135 ka reflects considerable erosion of valley-fill deposits in the plateau interior (Munack et al., 2016). In contrast, provenance data here indicate limited contribution of Rupshu Plateau sediments to the modern sediment budget since 8 ka. These valley fills were most likely eroded before the mid-Holocene, and since then they have been insignificant to the net sediment budget.

To assess how erosion of valley fills from the Zanskar River might contribute to regional upper Indus River sediment budgets over longer time scales, average yield rates over several possible residence intervals—10, 20, and 135 ka (Table 5)—were calculated. Yield rates for the last 10 ka were estimated at 89–279 $t/km^2/yr$ based on eroded sediment budgets derived from field observations of terrace height and incised width (Clift and Giosan, 2014). If these eroded budgets are accurate, then the pre-Holocene total stored sediment volume would have reached ~45–60 km^3. This suggests that ~42–77% of stored Zanskar River sediments (excluding the Rupshu Plateau) have been excavated and transported to the trunk Indus River since 10 ka.

Blöthe and Korup (2013) estimated ~177 km^3 of stored valley fill in the upper Indus River basin. The Zanskar River basin comprises ~7% of the upper Indus drainage area and a moderate ~21% of the total stored volume, of which at least ~9% is available for modern erosion. We propose that the Zanskar River may have a disproportionate influence on upper Indus River sediment volumes and compositions, especially if neighboring Transhimalaya valley fills in the plateau interior are isolated like the Rupshu Plateau. Sufficient transport capacity might only be achieved during episodic high-precipitation intervals when previously isolated plateau interior valley fills are eroded significantly into the trunk Indus River. In this context, marginal rain shadow river basins, which equally produce and mobilize abundant sediment, can strongly modify the Himalayan rain shadow sediment budget. Yet this also underscores that Transhimalayan valley fills, although volumetrically significant, modulate the total Indus River sediment budget much less than previously envisaged (Blöthe and Korup, 2013; Clift and Giosan, 2014).

CONCLUSIONS

This study defines the episodic infilling of volumetrically large Quaternary valley fills within the Zanskar River basin, the largest tributary to the upper Indus River, and marks coherent shifts in downstream sediment provenance as valley fills were periodically dissected. A new river terrace chronology documents at least two major phases of late Pleistocene–early Holocene aggradation. The first phase at 32–25 ka correlates in part with local deglaciation and strong South Asian summer monsoon and winter westerlies–derived precipitation. A second phase of aggradation initiated before 12 ka and lasted until ~8 ka, coinciding again with a strengthening summer monsoon. Over this time, aggradation is similarly documented along the frontal Himalaya (Bookhagen et al., 2006). Net Holocene incision as the climate dried, accompanied by loess sedimentation, initiated by 7–6 ka and was likely continuous through the present. Much of the bedrock erosion is controlled directly by glaciers and periglacial frost cracking, which in turn are modulated by summer monsoon and winter westerlies precipitation. Results from this study support the concept that regions of the Transhimalaya lying immediately north of the topographic divide may not only be sensitive to abnormal monsoonal excursions (Bookhagen et al., 2005b), but also record strong monsoon phases over the last ~35 ka. This work

highlights the control of the monsoon in addition to glaciation in landscape evolution on the periphery of the Tibetan Plateau.

Data presented here identify ~37 km^3 of stored sediment in the modern Zanskar River, but only ~16 km^3 of this is readily erodible. These values are consistent with previously published budgets, despite being estimated by different methodologies. Zanskar River valley fills host ~18% of the total upper Indus River sediment (~177 km^3) in only ~7% of its drainage area but may disproportionately contribute to the total upper Indus budget during particular climatic regimes. If many Transhimalayan valley fills within the plateau interior are isolated from the trunk river and/or are without sufficient transport capacity, then sedimentary signals to the trunk upper Indus will be fluxed primarily from those basins on the margin and will not be representative for all sectors of the Transhimalaya.

Deconvolving sedimentary signals preserved in offshore archives strictly in terms of climate or tectonically driven erosion continues to be problematic because sediment buffering occurs over many spatial and temporal scales and is now documented to occur prolifically even within mountain source regions. This study indicates that climatically modulated sediment buffering has occurred over 10^3–10^4 yr time scales in the upper Indus River and locally presents biases in both sediment compositions and volumes that need to be accounted for when analyzing sequences deposited farther downstream. Climate, and in particular precipitation, governs Himalayan rain shadow erosion more strongly than previously recognized. This observation highlights that millennial-scale climate variations can strongly pace landscape evolution in arid mountain belts and even further regulate the long-term dissection and decay of orogenic plateaus.

ACKNOWLEDGMENTS

This study was supported by the Charles T. McCord Jr. Chair in petroleum geology at Louisiana State University (LSU) and in part by a Geological Society of America Graduate Student Research Grant and LSU scholarships. This manuscript was greatly improved by constructive reviews from Luca Malatesta and one anonymous reviewer. The authors thank Tom Stevens for one OSL analysis incorporated into this study from Royal Holloway University of London. TNJ and PDC thank Fida Hussein Mittoo and family with Rockland Tourism, and Arundeep Ahluwalia from Panjab University for logistical support. TNJ appreciates fruitful discussions with Henry Munack and Jan Blöthe about morphometric analysis in Ladakh.

SUPPLEMENTARY MATERIAL

To view supplementary material for this article, please visit https://doi.org/10.1017/qua.2017.92

REFERENCES

Alizai, A., Carter, A., Clift, P.D., VanLaningham, S., Williams, J.C., Kumar, R., 2011. Sediment provenance, reworking and transport processes in the Indus River by U–Pb dating of detrital zircon grains. *Global and Planetary Change* 76, 33–55.

Allen, P.A., 2008. Time scales of tectonic landscapes and their sediment routing systems. *Geological Society, London, Special Publications* 296, 7–28.

Allison, M., Kuehl, S., Martin, T., Hassan, A., 1998. Importance of flood-plain sedimentation for river sediment budgets and terrigenous input to the oceans: insights from the Brahmaputra-Jamuna River. *Geology* 26, 175–178.

Amidon, W.H., Burbank, D.W., Gehrels, G.E., 2005. U-Pb zircon ages as a sediment mixing tracer in the Nepal Himalaya. *Earth and Planetary Science Letters* 235, 244–260.

Armitage, J.J., Duller, R.A., Whittaker, A.C., Allen, P.A., 2011. Transformation of tectonic and climatic signals from source to sedimentary archive. *Nature Geoscience* 4, 231–235.

Bailey, R.M., Arnold, L.J., 2006. Statistical modelling of single grain quartz De distributions and an assessment of procedures for estimating burial dose. *Quaternary Science Reviews* 25, 2475–2502.

Bajracharya, S., Shrestha, F., Bajracharya, S., Maharjan, S., & Guo, W. 2014. GLIMS Glacier Database. Boulder, CO, (15 April 2015). National Snow and Ice Data Center. doi: http://dx.doi.org/10.7265/N5V98602.

Benn, D.I., Owen, L.A., 1998. The role of the Indian summer monsoon and the mid-latitude westerlies in Himalayan glaciation: review and speculative discussion. *Journal of the Geological Society* 155, 353–363.

Berger, A., Loutre, M.-F., 1991. Insolation values for the climate of the last 10 million years. *Quaternary Science Reviews* 10, 297–317.

Black, L.P., Kamo, S.L., Allen, C.M., Aleinikoff, J.N., Davis, D.W., Korsch, R.J., Foudoulis, C., 2003. TEMORA 1: a new zircon standard for Phanerozoic U-Pb geochronology. *Chemical Geology* 200, 155–170.

Blöthe, J.H., Korup, O., 2013. Millennial lag times in the Himalayan sediment routing system. *Earth and Planetary Science Letters* 382, 38–46.

Blöthe, J.H., Munack, H., Korup, O., Fülling, A., Garzanti, E., Resentini, A., Kubik, P.W., 2014. Late Quaternary valley infill and dissection in the Indus River, western Tibetan Plateau margin. *Quaternary Science Reviews* 94, 102–119.

Bolch, T., Kulkarni, A., Kääb, A., Huggel, C., Paul, F., Cogley, J.G., Frey, H., et al., 2012. The state and fate of Himalayan glaciers. *Science* 336, 310–314.

Bookhagen, B., Burbank, D.W., 2006. Topography, relief, and TRMM-derived rainfall variations along the Himalaya. *Geophysical Research Letters* 33, L08405. http://dx.doi.org/10.1029/2006GL026037.

Bookhagen, B., Burbank, D.W., 2010. Toward a complete Himalayan hydrological budget: spatiotemporal distribution of snowmelt and rainfall and their impact on river discharge. *Journal of Geophysical Research: Earth Surface* 115, F03019. http://dx.doi.org/10.1029/2009JF001426.

Bookhagen, B., Fleitmann, D., Nishiizumi, K., Strecker, M., Thiede, R., 2006. Holocene monsoonal dynamics and fluvial terrace formation in the northwest Himalaya, India. *Geology* 34, 601–604.

Bookhagen, B., Thiede, R.C., Strecker, M.R., 2005a. Abnormal monsoon years and their control on erosion and sediment flux in the high, arid northwest Himalaya. *Earth and Planetary Science Letters* 231, 131–146.

Bookhagen, B., Thiede, R.C., Strecker, M.R., 2005b. Late Quaternary intensified monsoon phases control landscape evolution in the northwest Himalaya. *Geology* 33, 149–152.

Bull, W.L., Knuepfer, P.L.K., 1987. Adjustments by the Charwell River, New Zealand, to uplift and climatic changes. *Geomorphology* 1, 15–32.

Burbank, D.W., Bookhagen, B., Gabet, E.J., Putkonen, J., 2012. Modern climate and erosion in the Himalaya. *Comptes Rendus Geoscience* 344, 610–626.

Burbank, D.W., Fort, M.B., 1985. Bedrock control on glacial limits: examples from the Ladakh and Zanskar ranges, north-western Himalaya, India. *Journal of Glaciology* 31, 143–149.

Castelltort, S., Van Den Driessche, J., 2003. How plausible are high-frequency sediment supply-driven cycles in the stratigraphic record? *Sedimentary Geology* 157, 3–13.

Cawood, P.A., Johnson, M.R., Nemchin, A.A., 2007. Early Palaeozoic orogenesis along the Indian margin of Gondwana: tectonic response to Gondwana assembly. *Earth and Planetary Science Letters* 255, 70–84.

Clift, P.D., 2006. Controls on the erosion of Cenozoic Asia and the flux of clastic sediment to the ocean. *Earth and Planetary Science Letters* 241, 571–580.

Clift, P.D., Carter, A., Krol, M., Kirby, E., 2002. Constraints on India-Eurasia collision in the Arabian Sea region taken from the Indus Group, Ladakh Himalaya, India. In: Clift, P.D., Kroon, D., Gaedicke, C., Craig, J. (Eds.), The Tectonic and Climatic Evolution of the Arabian Sea Region. *Geological Society. London, Special Publications* 195, 97–116.

Clift, P.D., Giosan, L., 2014. Sediment fluxes and buffering in the post-glacial Indus Basin. *Basin Research* 26, 369–386.

Clift, P.D., Giosan, L., Blusztajn, J., Campbell, I.H., Allen, C.M., Pringle, M., Tabrez, A., et al., 2008. Holocene erosion of the Lesser Himalaya triggered by intensified summer monsoon. *Geology* 36, 79–82.

Clift, P.D., Plumb, R.A., 2008. The Asian Monsoon: Causes, History and Effects. Cambridge University Press, Cambridge.

Clift, P.D., Shimizu, N., Layne, G.D., Blusztajn, J.S., Gaedicke, C., Schlüter, H.U., Clark, M.K., Amjad, S., 2001. Development of the Indus Fan and its significance for the erosional history of the western Himalaya and Karakoram. *Geological Society of America Bulletin* 113, 1039–1051.

Demske, D., Tarasov, P.E., Wünnemann, B., Riedel, F., 2009. Late glacial and Holocene vegetation, Indian monsoon and westerly circulation in the Trans-Himalaya recorded in the lacustrine pollen sequence from Tso Kar, Ladakh, NW India. *Palaeogeography, Palaeoclimatology, Palaeoecology* 279, 172–185.

Dey, S., Thiede, R.C., Schildgen, T.F., Wittmann, H., Bookhagen, B., Scherler, D., Jain, V., Strecker, M.R., 2016. Climate-driven sediment aggradation and incision since the late Pleistocene in the NW Himalaya, India. *Earth and Planetary Science Letters* 449, 321–331.

Dèzes, P.J., Vannay, J.C., Steck, A., Bussy, F., Cosca, M., 1999. Synorogenic extension: quantitative constraints on the age and displacement of the Zanskar shear zone (northwest Himalaya). *Geological Society of America Bulletin* 111, 364–374.

Dietsch, C., Dortch, J.M., Reynhout, S.A., Owen, L.A., Caffee, M.W., 2015. Very slow erosion rates and landscape preservation across the southwestern slope of the Ladakh Range, India. *Earth Surface Processes and Landforms* 40, 389–402.

Dortch, J.M., Dietsch, C., Owen, L.A., Caffee, M.W., Ruppert, K., 2011. Episodic fluvial incision of rivers and rock uplift in the Himalaya and Transhimalaya. *Journal of the Geological Society* 168, 783–804.

Dortch, J.M., Owen, L.A., Caffee, M.W., 2010. Quaternary glaciation in the Nubra and Shyok valley confluence, northernmost Ladakh, India. *Quaternary Research* 74, 132–144.

Dortch, J.M., Owen, L.A., Caffee, M.W., 2013. Timing and climatic drivers for glaciation across semi-arid western Himalayan–Tibetan orogen. *Quaternary Science Reviews* 78, 188–208.

Duller, G.A.T., 2008. Single-grain optical dating of Quaternary sediments: why aliquot size matters in luminescence dating. *Boreas* 37, 589–612.

Dutt, S., Gupta, A.K., Clemens, S.C., Cheng, H., Singh, R.K., Kathayat, G., Edwards, R.L., 2015. Abrupt changes in Indian summer monsoon strength during 33,800 to 5500 years BP. *Geophysical Research Letters* 42, 5526–5532.

Epard, J.-L., Steck, A., 2008. Structural development of the Tso Morari ultra-high pressure nappe of the Ladakh Himalaya. *Tectonophysics* 451, 242–264.

Fang, J., 1991. Lake evolution during the past 30,000 years in China, and its implications for environmental change. *Quaternary Research* 36, 37–60.

Fleitmann, D., Burns, S.J., Mudelsee, M., Neff, U., Kramers, J., Mangini, A., Matter, A., 2003. Holocene forcing of the Indian monsoon recorded in a stalagmite from southern Oman. *Science* 300, 1737–1739.

Fuchs, G., 1986. The geology of the Markha-Khurnak region in Ladakh (India). *Jahrbuch der Geologischen Bundesanstalt Wien* 128, 403–437.

Fuchs, G., 1987. The geology of southern Zanskar (Ladakh) – evidence for the autochthony of the Tethys Zone of the Himalaya. *Jahrbuch der Geologischen Bundesanstalt Wien* 130, 465–491.

Gabet, E.J., Burbank, D.W., Pratt-Sitaula, B., Putkonen, J., Bookhagen, B., 2008. Modern erosion rates in the High Himalayas of Nepal. *Earth and Planetary Science Letters* 267, 482–494.

Galy, A., France-Lanord, C., 2001. Higher erosion rates in the Himalaya: geochemical constraints on riverine fluxes. *Geology* 29, 23–26.

Garzanti, E., Andò, S., 2007a. Heavy mineral concentration in modern sands: implications for provenance interpretation. In: Mange, M.A., Wright, D.T. (Eds.), *Heavy Minerals in Use*. Elsevier, Amsterdam, pp. 517–545.

Garzanti, E., Andò, S., 2007b. Plate tectonics and heavy mineral suites of modern sands. In: Mange, M.A., Wright, D.T. (Eds.), *Heavy Minerals in Use*. Elsevier, Amsterdam, pp. 741–763.

Garzanti, E., Vezzoli, G., 2003. A classification of metamorphic grains in sands based on their composition and grade. *Journal of Sedimentary Research* 73, 830–837.

Gasse, F., Arnold, M., Fontes, J.C., Fort, M., Gibert, E., Huc, A., Bingyan, L., Yuanfang, L., Qing, L., Melieres, F., 1991. A 13,000-year climate record from western Tibet. *Nature* 353, 742–745.

Gasse, F., Fontes, J.C., Van Campo, E., Wei, K., 1996. Holocene environmental changes in Bangong Co basin (western Tibet). Part 4: discussion and conclusions. *Palaeogeography, Palaeoclimatology, Palaeoecology* 120, 79–92.

Gehrels, G.E., 2014. Detrital zircon U-Pb geochronology applied to tectonics. *Annual Review of Earth and Planetary Sciences* 42, 127–149.

Giosan, L., Clift, P.D., Macklin, M.G., Fuller, D.Q., Constantinescu, S., Durcan, J.A., Stevens, T., et al., 2012. Fluvial landscapes of the

Harappan civilization. *Proceedings of the National Academy of Sciences of the United States of America* 109, E1688–E1694.
Goodbred, S.L., 2003. Response of the Ganges dispersal system to climate change: a source-to-sink view since the last interstade. *Sedimentary Geology* 162, 83–104.
Griffin, W.L., Powell, W.J., Pearson, N.J., O'Reilly, S.Y., 2008. GLITTER: data reduction software for laser ablation ICP-MS. In: Sylvester, P. (Ed.), Laser Ablation ICP-MS in the Earth Sciences. Mineralogical Association of Canada Short Course Series 40. Mineralogical Association of Canada, Ottawa, pp. 204–207.
Gupta, A.K., Anderson, D.M., Overpeck, J.T., 2003. Abrupt changes in the Asian southwest monsoon during the Holocene and their links to North Atlantic Ocean. *Nature* 421, 354–357.
Hales, T.C., Roering, J.J., 2005. Climate-controlled variations in scree production, Southern Alps, New Zealand. *Geology* 33, 701–704.
Hales, T.C, Roering, J.J., 2007. Climatic controls on frost cracking and implications for the evolution of bedrock landscapes. *Journal of Geophysical Research: Earth Surface* 112, F02033. http://dx.doi.org/10.1029/2006JF000616.
Hartmann, H., 1987. Pflanzengesellschaften trockener Standorte aus der subalpinen und alpinen Stufe im südlichen und östlichen Ladakh. *Candollea* 42, 277–326.
Hedrick, K.A., Owen, L.A., Chen, J., Robinson, A., Yuan, Z., Yang, X., Imrecke, D.B., et al., 2017. Quaternary history and landscape evolution of a high-altitude intermountain basin at the western end of the Himalayan-Tibetan orogen, Waqia Valley, Chinese Pamir. *Geomorphology* 284, 156–174.
Hedrick, K.A., Seong, Y.B., Owen, L.A., Caffee, M.W., Dietsch, C., 2011. Towards defining the transition in style and timing of Quaternary glaciation between the monsoon-influenced Greater Himalaya and the semi-arid Transhimalaya of northern India. *Quaternary International* 236, 21–33.
Henderson, A.L., Najman, Y., Parrish, R., BouDagher-Fadel, M., Barford, D., Garzanti, E., Andò, S., 2010. Geology of the Cenozoic Indus Basin sedimentary rocks: paleoenvironmental interpretation of sedimentation from the western Himalaya during the early phases of India-Eurasia collision. *Tectonics* 29, TC6015. http://dx.doi.org/10.1029/2009TC002651.
Herren, E., 1987. Zanskar shear zone: northeast-southwest extension within the Higher Himalayas (Ladakh, India). *Geology* 15, 409–413.
Herzschuh, U., 2006. Palaeo-moisture evolution in monsoonal Central Asia during the last 50,000 years. *Quaternary Science Reviews* 25, 163–178.
Hewitt, K., 1998. Catastrophic landslides and their effects on the Upper Indus streams, Karakoram Himalaya, northern Pakistan. *Geomorphology* 26, 47–80.
Hewitt, K., 2002. Postglacial landform and sediment associations in a landslide-fragmented river system: the Transhimalayan Indus streams, Central Asia. In: Hewitt, K., Byrne, M.-L., English, M., Young, G. (Eds.), Landscapes of Transition: Landform Assemblages and Transformations in Cold Regions. Springer, Dordrecht, the Netherlands, pp. 63–91.
Hobley, D.E., Sinclair, H.D., Mudd, S.M., 2012. Reconstruction of a major storm event from its geomorphic signature: the Ladakh floods, 6 August 2010. *Geology* 40, 483–486.
Honegger, K., Dietrich, V., Frank, W., Gansser, A., Thöni, M., Trommsdorff, V., 1982. Magmatism and metamorphism in the Ladakh Himalayas (the Indus-Tsangpo suture zone). *Earth and Planetary Science Letters* 60, 253–292.
Horton, F., Lee, J., Hacker, B., Bowman-Kamaha'o, M., Cosca, M., 2015. Himalayan gneiss dome formation in the middle crust and exhumation by normal faulting: new geochronology of Gianbul dome, northwestern India. *Geological Society of America Bulletin* 127, 162–180.
Horton, F., Leech, M.L., 2013. Age and origin of granites in the Karakoram shear zone and Greater Himalaya Sequence, NW India. *Lithosphere* 5, 300–320.
Ingersoll, R.V., Bullard, T.F., Ford, R.L., Grimm, J.P., Pickle, J.D., Sares, S.W., 1984. The effect of grain size on detrital modes: a test of the Gazzi-Dickinson point-counting method. *Journal of Sedimentary Petrology* 54, 103–116.
Jade, S., Rao, H.J.R., Vijayan, M.S.M., Gaur, V.K., Bhatt, B.C., Kumar, K., Jaganathan, S., Ananda, M.B., Kumar, P.D., 2010. GPS-derived deformation rates in northwestern Himalaya and Ladakh. *International Journal of Earth Sciences* 100, 1293–1301.
Jaiswal, M., Srivastava, P., Tripathi, J., Islam, R., 2008. Feasibility of the SAR technique on Quartz sand of terraces of NW Himalaya: a case study from Devprayag. *Geochronometria* 31, 45–52.
Jerolmack, D.J., Paola, C., 2010. Shredding of environmental signals by sediment transport. *Geophysical Research Letters* 37, L19401. http://dx.doi.org/10.1029/2010GL044638.
Jonell, T.N., Carter, A., Böning, P., Pahnke, K., Clift, P.D., 2017. Climatic and glacial impact on erosion patterns and sediment provenance in the Himalayan rain shadow, Zanskar River, NW India. *Geological Society of America Bulletin* 129, 820–836.
Kamp, U., Byrne, M., Bolch, T., 2011. Glacier fluctuations between 1975 and 2008 in the Greater Himalaya Range of Zanskar, southern Ladakh. *Journal of Mountain Science* 8, 374–389.
Kathayat, G., Cheng, H., Sinha, A., Spötl, C., Edwards, R.L., Zhang, H., Li, X., Yi, L., Ning, Y., Cai, Y., 2016. Indian monsoon variability on millennial-orbital timescales. *Scientific Reports* 6, 24374. http://dx.doi.org/10.1038/srep24374.
Kirstein, L.A., Foeken, J.P.T., Van Der Beek, P., Stuart, F.M., Phillips, R.J., 2009. Cenozoic unroofing history of the Ladakh Batholith, western Himalaya, constrained by thermochronology and numerical modelling. *Journal of the Geological Society* 166, 667–678.
Kirstein, L.A., Sinclair, H.D., Stuart, F.M., Dobson, K., 2006. Rapid early Miocene exhumation of the Ladakh batholith, western Himalaya. *Geology* 34, 1049–1052.
Korup, O., Montgomery, D.R., Hewitt, K., 2010. Glacier and landslide feedbacks to topographic relief in the Himalayan syntaxes. *Proceedings of the National Academy of Sciences of the United States of America* 107, 5317–5322.
Kumar, A., Srivastava, P., Meena, N.K., 2017. Late Pleistocene aeolian activity in the cold desert of Ladakh: a record from sand ramps. *Quaternary International* 443, 13–28.
Lee, S.Y., Seong, Y.B., Owen, L.A., Murari, M.K., Lim, H.S., Yoon, H.I., Yoo, K.C., 2014. Late Quaternary glaciation in the Nun-Kun massif, northwestern India. *Boreas* 43, 67–89.
Leipe, C., Demske, D., Tarasov, P.E., 2014. A Holocene pollen record from the northwestern Himalayan lake Tso Moriri: implications for palaeoclimatic and archaeological research. *Quaternary International* 348, 93–112.
Métivier, F., Gaudemer, Y., 1999. Stability of output fluxes of large rivers in South and East Asia during the last 2 million years: implications on floodplain processes. *Basin Research* 11, 293–303.

Mishra, P.K., Anoop, A., Schettler, G., Prasad, S., Jehangir, A., Menzel, P., Naumann, R., Yousuf, A., Basavaiah, N., Deenadayalan, K., 2015. Reconstructed late Quaternary hydrological changes from Lake Tso Moriri, NW Himalaya. *Quaternary International* 371, 76–86.

Mitchell, W.A., Taylor, P.J., Osmaston, H., 1999. Quaternary geology in Znaskar, NW Indian Himalaya: evidence for restricted glaciation and preglacial topography. *Journal of Asian Earth Sciences* 17, 307–318.

Munack, H., Blöthe, J.H., Fülöp, R.H., Codilean, A.T., Fink, D., Korup, O., 2016. Recycling of Pleistocene valley fills dominates 135 ka of sediment flux, upper Indus River. *Quaternary Science Reviews* 149, 122–134.

Murari, M.K., Owen, L.A., Dortch, J.M., Caffee, M.W., Dietsch, C., Fuchs, M., Haneberg, W.C., Sharma, M.C., Townsend-Small, A., 2014. Timing and climatic drivers for glaciation across monsoon-influenced regions of the Himalayan–Tibetan orogen. *Quaternary Science Reviews* 88, 159–182.

Nie, J., Stevens, T., Rittner, M., Stockli, D., Garzanti, E., Limonta, M., Bird, A., et al., 2015. Loess Plateau storage of northeastern Tibetan Plateau–derived Yellow River sediment. Nature. *Communications* 6, 8511. http://dx.doi.org/10.1038/ncomms9511.

Noble, S.R., Searle, M.P., 1995. Age of crustal melting and leukogranite formation from U-Pb zircon and monazite dating in the western Himalaya, Zanskar, India. *Geology* 23, 1135–1138.

Osmaston, H., 1994. The geology, geomorphology and Quaternary history of Zangskar. In: Crook, J., Osmaston, H. (Ed.), Himalayan Buddhist Villages: Environment, Resources, Society and Religious Life in Zangskar, Ladakh. University of Bristol, Bristol, UK, pp. 1–35.

Owen, L.A., 2009. Latest Pleistocene and Holocene glacier fluctuations in the Himalaya and Tibet. *Quaternary Science Reviews* 28, 2150–2164.

Owen, L.A., Caffee, M.W., Bovard, K.R., Finkel, R.C., Sharma, M.C., 2006. Terrestrial cosmogenic nuclide surface exposure dating of the oldest glacial successions in the Himalayan orogen: Ladakh Range, northern India. *Geological Society of America Bulletin* 118, 383–392.

Owen, L.A., Dortch, J.M., 2014. Nature and timing of Quaternary glaciation in the Himalayan–Tibetan orogen. *Quaternary Science Reviews* 88, 14–54.

Owen, L.A., Gualtieri, L., Finkel, R.C., Caffee, M.W., Benn, D.I., Sharma, M.C., 2002. Reply: cosmogenic radionuclide dating of glacial landforms in the Lahul Himalaya, northern India: defining the timing of Late Quaternary glaciation. *Journal of Quaternary Science* 17, 279–281.

Pant, R., Phadtare, N., Chamyal, L., Juyal, N., 2005. Quaternary deposits in Ladakh and Karakoram Himalaya: a treasure trove of the palaeoclimate records. *Current Science* 88, 1789–1798.

Phartiyal, B., Sharma, A., Upadhyay, R., 2005. Quaternary geology, tectonics and distribution of palaeo- and present fluvio/glacio lacustrine deposits in Ladakh, NW Indian Himalaya—a study based on field observations. *Geomorphology* 65, 241–256.

Pognante, U., Castelli, D., Benna, P., Genovese, G., Oberli, F., Meier, M., Tonarini, S., 1990. The crystalline units of the High Himalayas in the Lahul-Zanskar region (northwest India): metamorphictectonic history and geochronology of the collided and imbricated Indian plate. *Geological Magazine* 127, 101–116.

Pratt, B., Burbank, D.W., Heimsath, A., Ojha, T., 2002. Impulsive alluviation during early Holocene strengthened monsoons, central Nepal Himalaya. *Geology* 30, 911–914.

Prescott, J.R., Hutton, J.T., 1994. Cosmic ray contributions to dose rates for luminescence and ESR dating: large depths and long-term time variations. *Radiation measurements* 23, 497–500.

Prins, M., Postma, G., Weltje, G.J., 2000. Controls on terrigenous sediment supply to the Arabian Sea during the late Quaternary: the Makran continental slope. *Marine Geology* 169, 351–371.

Rhodes, E.J., 2011. Optically stimulated luminescence dating of sediments over the past 200,000 years. *Annual Review of Earth and Planetary Sciences* 39, 461–488.

Romans, B.W., Castelltort, S., Covault, J.A., Fildani, A., Walsh, J., 2016. Environmental signal propagation in sedimentary systems across timescales. *Earth-Science Reviews* 153, 7–29.

Saha, S., Sharma, M.C., Murari, M.K., Owen, L.A., Caffee, M.W., 2016. Geomorphology, sedimentology and minimum exposure ages of streamlined subglacial landforms in the NW Himalaya, India. *Boreas* 45, 284–303.

Schaetzl, R.J., Forman, S.L., 2008. OSL ages on glaciofluvial sediment in northern Lower Michigan constrain expansion of the Laurentide ice sheet. *Quaternary Research* 70, 81–90.

Scherler, D., Bookhagen, B., Wulf, H., Preusser, F., Strecker, M.R., 2015. Increased late Pleistocene erosion rates during fluvial aggradation in the Garhwal Himalaya, northern India. *Earth and Planetary Science Letters* 428, 255–266.

Scherler, D., Munack, H., Mey, J., Eugster, P., Wittmann, H., Codilean, A.T., Kubik, P., Strecker, M.R., 2014. Ice dams, outburst floods, and glacial incision at the western margin of the Tibetan Plateau: a >100 k.y. chronology from the Shyok Valley, Karakoram. *Geological Society of America Bulletin* 126, 738–758.

Schlup, M., Carter, A., Cosca, M., Steck, A., 2003. Exhumation history of eastern Ladakh revealed by ^{40}Ar-^{39}Ar and fission track ages: the Indus River–Tso Morari transect, NW Himalaya. *Journal of the Geological Society* 160, 385–399.

Schlup, M., Steck, A., Carter, A., Cosca, M., Epard, J.-L., Hunziker, J., 2011. Exhumation history of the NW Indian Himalaya revealed by fission track and ^{40}Ar/^{39}Ar ages. *Journal of Asian Earth Sciences* 40, 334–350.

Schwanghart, W., Scherler, D., 2014. Short Communication: TopoToolbox 2 – MATLAB-based software for topographic analysis and modeling in Earth surface sciences. *Earth Surface Dynamics* 2, 1–7.

Searle, M.P., 1983. On the Tectonics of the Western Himalaya. *Episodes* 1983, 21–26.

Searle, M.P., Pickering, K.T., Cooper, D.J.W., 1990. Restoration and evolution of the intermontane Indus molasse basin, Ladakh Himalaya, India. *Tectonophysics* 174, 301–314.

Sharma, S., Chand, P., Bisht, P., Shukla, A.D., Bartarya, S., Sundriyal, Y., Juyal, N., 2016. Factors responsible for driving the glaciation in the Sarchu Plain, eastern Zanskar Himalaya, during the late Quaternary. *Journal of Quaternary Science* 31, 495–511.

Shellnutt, J.G., Bhat, G.M., Wang, K.-L., Brookfield, M.E., Dostal, J., Jahn, B.-M., 2012. Origin of the silicic volcanic rocks of the Early Permian Panjal Traps, Kashmir, India. *Chemical Geology* 334, 154–170.

Shellnutt, J.G., Bhat, G.M., Wang, K.-L., Brookfield, M.E., Jahn, B.-M., Dostal, J., 2014. Petrogenesis of the flood basalts from the Early Permian Panjal Traps, Kashmir, India: geochemical evidence for shallow melting of the mantle. *Lithos* 204, 159–171.

Shi, Y., Yu, G., Liu, X., Li, B., Yao, T., 2001. Reconstruction of the 30–40 ka bp enhanced Indian monsoon climate based on

geological records from the Tibetan Plateau. *Palaeogeography, Palaeoclimatology, Palaeoecology* 169, 69–83.

Simpson, G., Castelltort, S., 2012. Model shows that rivers transmit high-frequency climate cycles to the sedimentary record. *Geology* 40, 1131–1134.

Sinha, A., Cannariato, K.G., Stott, L.D., Li, H.-C., You, C.-F., Cheng, H., Edwards, R.L., Singh, I.B., 2005. Variability of southwest Indian summer monsoon precipitation during the Bølling-Ållerød. *Geology* 33, 813–816.

Sláma, J., Košler, J., Condon, D.J., Crowley, J.L., Gerdes, A., Hanchar, J.M., Horstwood, M.S.A., et al., 2008. Plešovice zircon—a new natural reference material for U–Pb and Hf isotopic microanalysis. *Chemical Geology* 249, 1–35.

Spring, L., Bussy, F., Vannay, J.-C., Huon, S., Cosca, M., 1993. Early Permian granitic dykes of alkaline affinity in the Indian High Himalaya of Upper Lahul and SE Zanskar: geochemical characterization and geotectonic implications. *Geological Society, London, Special Publications* 74, 251–264.

Srivastava, P., Rajak, M.K., Singh, L.P., 2009. Late Quaternary alluvial fans and paleosols of the Kangra basin, NW Himalaya: tectonic and paleoclimatic implications. *Catena* 76, 135–154.

Srivastava, P., Tripathi, J.K., Islam, R., Jaiswal, M.K., 2008. Fashion and phases of Late Pleistocene aggradation and incision in Alaknanda River, western Himalaya India. *Quaternary Research* 70, 68–80.

Staubwasser, M., Weiss, H., 2006. Holocene climate and cultural evolution in late prehistoric–early historic West Asia. *Quaternary Research* 66, 372–387.

Steck, A., Spring, L., Vannay, J.-C., Masson, H., Stutz, E., Bucher, H., Marchant, R., Tièche, J.-C., 1993. Geological transect across the northwestern Himalaya in eastern Ladakh and Lahul (a model for the continental collision of India and Asia). *Eclogae Geologicae Helvetiae* 86, 219–263.

Taylor, P.J., Mitchell, W.A., 2000. The Quaternary glacial history of the Zanskar range, north-west Indian Himalaya. *Quaternary International* 65–66, 81–99.

Thakur, V., Joshi, M., Sahoo, D., Suresh, N., Jayangondapermal, R., Singh, A., 2014. Partitioning of convergence in northwest sub-Himalaya: estimation of late Quaternary uplift and convergence rates across the Kangra reentrant, north India. *International Journal of Earth Sciences* 103, 1037–1056.

Vermeesch, P., 2004. How many grains are needed for a provenance study? *Earth and Planetary Science Letters* 224, 351–441.

Vermeesch, P., 2012. On the visualisation of detrital age distributions. *Chemical Geology* 312–313, 190–194.

Vermeesch, P., Resentini, A., Garzanti, E., 2016. An R package for statistical provenance analysis. *Sedimentary Geology* 336, 14–25.

Walder, J., Hallet, B., 1985. A theoretical model of the fracture of rock during freezing. *Geological Society of America Bulletin* 96, 336–346.

Wiedenbeck, M., Hanchar, J.M., Peck, W.H., Sylvester, P., Valley, J., Whitehouse, M., Kronz, A., et al., 2004. Further characterisation of the 91500 zircon crystal. *Geostandards and Geoanalytical Research* 28, 9–39.

Wintle, A.G., Murray, A.S., 2006. A review of quartz optically stimulated luminescence characteristics and their relevance in single-aliquot regeneration dating protocols. *Radiation Measurements* 41, 369–391.

Wulf, H., Bookhagen, B., Scherler, D., 2010. Seasonal precipitation gradients and their impact on fluvial sediment flux in the northwest Himalaya. *Geomorphology* 118, 13–21.

Wulf, H., Bookhagen, B., Scherler, D., 2012. Climatic and geologic controls on suspended sediment flux in the Sutlej River Valley, western Himalaya. *Hydrology and Earth System Sciences Discussions* 9, 541–594.

Wünnemann, B., Demske, D., Tarasov, P., Kotlia, B.S., Reinhardt, C., Bloemendal, J., Diekmann, B., et al., 2010. Hydrological evolution during the last 15 kyr in the Tso Kar lake basin (Ladakh, India), derived from geomorphological, sedimentological and palynological records. *Quaternary Science Reviews* 29, 1138–1155.

Yang, S., Zhang, F., Wang, Z., 2012. Grain size distribution and age population of detrital zircons from the Changjiang (Yangtze) River system, China. *Chemical Geology* 296–297, 26–38.